REPORT DOCUMENTATION PAGE

Form Approved
OMB NO. 0704-0188

1. AGENCY USE ONLY (Leave Blank)	2. REPORT DATE	3. REPORT TYPE AND DATES COVERED
	31 Jul 98	Final Report 1 Aug 97 -- 30 Jun 98

4. TITLE AND SUBTITLE
Reliability-Based Modeling and Analysis of Advanced Composites. Phase I Final Report

5. FUNDING NUMBERS
DAAG55-97-C-0053

6. AUTHOR(S)
R. G. Tryon, A. Dey, S. Mahadevan, Y. Wang, C. Q. Rousseau

7. PERFORMING ORGANIZATION NAME(S) AND ADDRESS(ES)
PerSyst Development Group of Paul Holland & Associates
5123 Virginia Way, Suite C-21
Brentwood, TN 37027

8. PERFORMING ORGANIZATION REPORT NUMBER
CR-PDG-STTR-97-0001-F

9. SPONSORING / MONITORING AGENCY NAME(S) AND ADDRESS(ES)
U. S. Army Research Office
P.O. Box 12211
Research Triangle Park, NC 27709-2211

10. SPONSORING / MONITORING AGENCY REPORT NUMBER
ARO 37448.1-EG-STI

11. SUPPLEMENTARY NOTES
The views, opinions and/or findings contained in this report are those of the author(s) and should not be construed as an official Department of the Army position, policy or decision, unless so designated by the documentation.

12 a. DISTRIBUTION / AVAILABILITY STATEMENT
Approved for public release; distribution unlimited

12 b. DISTRIBUTION CODE

13. ABSTRACT (Maximum 200 words)

The objective of the Phase I effort was to incorporate high performance composite design methodologies with mechanistic failure models to predict the reliability of composite structures. The methodology was demonstrated on a helicopter rotor hub tapered test specimen. The specimen is subjected to a static axial load and an oscillatory angular displacement. The observed failure mechanism is an initial tension crack followed by internal delamination. The research effort developed a non-linear structural model of the rotor hub using the finite element program ANSYS in which the internal plies and the delamination were explicitly modeled. The output from structural model was fed into the Virtual Crack Closure Technique (VCCT) module to predict the strain energy that is required to cause delamination onset. The response surface analysis was used to develop a limit state equation relating the primitive input design variables to strain energy release rate. A Reliability Analysis framework using first order reliability method (FORM) was developed and integrated with the structural analysis modules. The FORM analysis estimated the probability of delamination onset as a function of cyclic lives and the relative importance of the primitive variables. Advanced mean value methods were also added to the reliability framework.

14. SUBJECT TERMS	15. NUMBER OF PAGES
STTR Report, Tapered Composites, Rotorcraft, First Order Reliability Method, Response Surface, Fatigue, Virtual Crack Closer Methods, Finite Element Method	52
	16. PRICE CODE

17. SECURITY CLASSIFICATION OF REPORT	18. SECURITY CLASSIFICATION ON THIS PAGE	19. SECURITY CLASSIFICATION OF ABSTRACT	20. LIMITATION OF ABSTRACT
UNCLASSIFIED	UNCLASSIFIED	UNCLASSIFIED	UL

Table of Content

Table of Figures

Table of Tables

1 Overview of the Research Effort

The objective of the current research is to develop a probabilistic analysis framework incorporating high performance composite design methodologies to predict the reliability of composite structures. The research links state-of-the-art laminate design techniques with failure models. This effort has the potential for application to the types of engineering tasks that are required for the development of new rotorcraft using modern composite materials and technologies and is especially relevant to the areas of damage tolerance and crash-worthiness. The research will yield a methodology and software that would greatly improve both our physical understanding and analytical capability in this subject area.

The methodology is being demonstrated on a helicopter rotor hub test specimen with thick, thin, and tapered regions. The specimen is subjected to a static axial load P and an oscillatory angular displacement Φ. The failure mechanism that is observed from this type of fatigue loading is an initial tension crack followed by internal delamination at the thick to taper transition where internal ply drop-offs occur.

A structural model of the rotor hub was created using the finite element program ANSYS. The output from the structural analysis in ANSYS was fed into the Virtual Crack Closure Technique (VCCT) module to model delamination onset. A Reliability Analysis framework including Response Surface Analysis and FORM modules was developed to integrate with the structural analysis modules. The response surface analysis was used to develop a limit state equation relating the primitive input design parameters (random variables such as P, and Φ) to strain energy release rate G_{max}. FORM analysis estimated the probability of delamination onset and furthermore, determined the distribution of the failure probability over a range of cyclic lives. In addition, the sensitivity analysis in FORM revealed that the external loading to the structure, namely P and Φ are the most critical parameters affecting the reliability of the rotor hub. Summarizing, the following tasks were successfully completed at the end of Phase I.

- Demonstrated probabilistic analysis framework
- Demonstrated composite Finite Element modeling (FEM) technique
- Developed framework for integrating probabilistic and FEM codes
- Applied developed method to a practical problem

Phase I of the proposed research effort has successfully demonstrated that the probabilistic analysis framework can be integrated with current state-of-the-art composite design to estimate the failure probability due to various critical failure modes. In addition, the same framework can be used to compute the sensitivity of the reliability of the final design to the random variables without any extra computational effort.

2 Identification and Significance of the Problem

The structural evaluation of composite materials is different from that used in isotropic materials. Behavior of composites is dependent on the specific way in which a given composite is layered. The orientations allow the designer freedom in tailoring structures for obtaining the desired response. The evaluation of composite structures needs to account for the effects of tailoring.

The development of advanced high-performance composites, until now, has mainly focused in achieving high modulus and high strength. But along with the high strength, such materials must also be able to absorb energy and resist cyclic fatigue loads. Fatigue loads can initiate progressive failure in a composite laminate by way of successive delamination, matrix cracking, fiber waviness, etc. Such imperfections can severely reduce the load carrying capacity of the laminates, ultimately leading to structural failure. While it is possible to address the effect of geometric and material non-linearity using current sophisticated analysis methods, the

highly stochastic nature of damage progression and extreme sensitivity to small geometrical uncertainties results in untrustworthy analytical predictions.

The problem is further compounded by the fact that there is significant randomness in the material and geometric properties of such composites. Another vital source of variance is the loads to which composite structures are subjected. The exact load distribution, its variation in time and therefore, its structural effect on composites for aerostructure applications are seldom deterministic. A probabilistic analysis framework incorporating the current laminate design methodologies is the best strategy to account for these variations in both load and material properties.

3 Technical Objectives of the Phase I Effort

The research developed a probabilistic analysis framework incorporating current aerostructure industry composite laminate design methodologies to predict the reliability of composite structures. The research considered the reliability-based composite design methodology as being divided into two distinct but closely coupled modeling techniques. The first modeling technique is the structural model that uses finite element analysis to determine the global and ply level response of the structure at the damage sites. The finite element analysis is the same as that currently employed in the aerostructure industry. The finite element model is extended to address the random nature of the structural application. The model considers the stochastic aspects of the input loads. Variation in the global geometry is considered, along with local ply level variation. The distributions of geometric variations were determined by investigating the sources of the variations such as standard manufacturing techniques, manufacturing anomalies, and service duty.

The second modeling techniques are the failure models that are closely coupled with the structural model. The failure models, which address initial damage, are specific models that have been developed by the rotorcraft industry and the Army Research Laboratory. The failure models consider many of the same input variations as the structural models. The failure models also consider variations in the local responses to determine the probability of occurrence of damage states.

The objective of the Phase I research was to develop and validate an overall progressive failure methodology using the approach outlined above.

4 Research Team

The research team comprises of PerSyst Development, Vanderbilt University and Bell Helicopter. For the probabilistic methodologies to have commercial application, these methodologies must be developed with a thorough understanding of current rotorcraft design practices. Thus, a close working relationship has been fostered between PerSyst/Vanderbilt and Bell Helicopter. Bell has identified rotor fatigue loading as a significant probabilistic design consideration due to the large amount of scatter in the observed fatigue life of the large scale composite rotor test specimens. The Phase I effort is targeted at developing and applying the probabilistic methodology to the design and analysis of the rotor test specimens currently used by Bell. The finite element-based macrostructural model is consistent with current modeling methods used at Bell and the microstructural fatigue damage accumulation model is based on the models developed through the cooperative efforts of Bell and the U.S. Army Research Laboratory. Bell is also helping the PerSyst/Vanderbilt team identify the work that must be completed in the Phase II effort. This collaboration will assure that the final product addresses the current and near term needs of composite rotorcraft design and assure that the final product can be successfully integrated into the design practice.

5 Phase I Research Conducted

The focus of the research has been in three areas; 1) determining the failure mechanism and developing the structural models to simulate the local conditions governing the failure mechanism for the demonstration problem, 2) developing the reliability computation framework for the demonstration problem and 3)

developing additional reliability algorithms. The focus areas have been further subdivided into several tasks. Each of these tasks is discussed below.

5.1 Focus Area 1: Failure Mechanisms and Models

5.1.1 Demonstration component

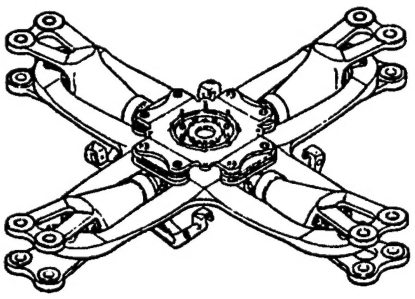

Figure 1: Rotor hub assembly.

Hingeless, bearingless helicopter rotor hubs are being designed using laminated composite materials to reduce weight, drag, and the number of parts in the hub as shown in Figure 1. An effective elastic hinge is designed integrally to the composite rotor yoke by incorporating a tapered region between thick and thin regions. The varying thickness of the tapered region is accomplished by dropping internal plies. The thick-taper-thin geometry is tailored to give the proper flapping flexure. An example of a composite rotor yoke is shown in Figure 2.

During flight, the rotor hub yoke experiences axial tension loads as well as bending loads. The axial tensile loads are centrifugal loads caused by the rotation of the rotor. The bending loads are caused by the interaction of the rotor passage with the fuselage or other static structures and aerodynamic gust loads. The actual load experience in service is a complex random spectrum dependent on mission, local environment, and turbulence [1].

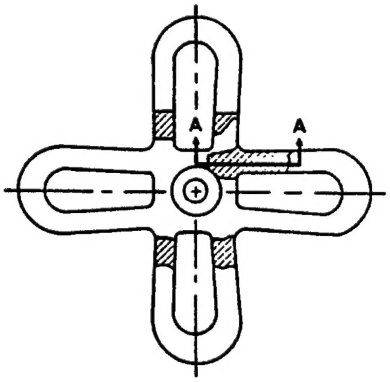

Figure 2: One-piece composite yoke.

Generalized test specimens have been developed to understand the basic response of the composite rotor hub yokes. The specimens are geometrically simple with thick, thin, and tapered regions, as shown in Figure 3 and approximate the geometry of section A-A in Figure 2. The specimens are subjected to constant axial tensile load (P) to simulate the rotation of the rotor at constant speed and cyclic bending load (V) to simulate the interaction of the rotor passage with the fuselage. A typical test setup is diagramed in Figure 3. The cyclic load (V) induces an angular displacement (θ) which simulates the flexural bending in the yoke.

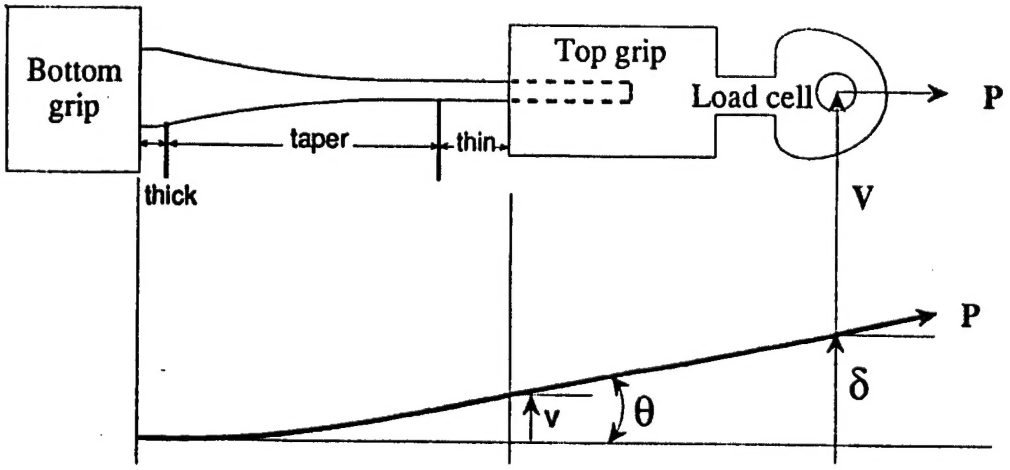

Figure 3: Typical test set-up.

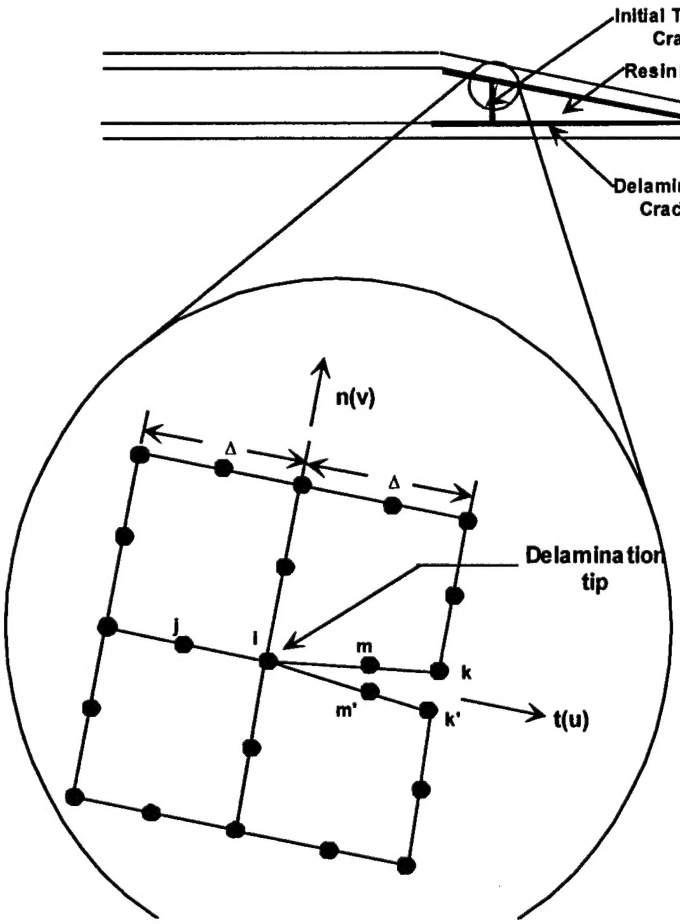

Figure 4: Model of crack tip at plydrop.

5.1.2 *Failure mechanism*

The plydrop in the laminate creates geometrical and material discontinuities that cause large interlaminar stresses and initiate delamination. The failure mechanism observed from this type of loading is an initial tension crack followed by internal delamination at the thick to taper transition where internal ply drop-offs occur.

5.1.3 *Failure model*

Several studies have investigated the effect of delamination failure in tapered laminates. Some of these studies have used stress-based criteria for modeling the failure [2-7]. Others have used a strain energy release rate approach to study delamination [8-13]. Most of the above mentioned methods have only considered delamination under pure tension, bending or torsion loads. Very few studies have considered the combined effect of bending and tension on delamination of tapered laminated composites [14,15].

In this study, the method used to model the delamination failure mechanism is based on total strain energy release rate G which is the sum of the mode I strain energy release rate and the mode II stain energy release rate. A virtual crack closure technique (VCCT) is used to calculated G at the delamination tip as shown in Figure 4 [16,17] such that

$$G = G_I + G_{II} \quad (4.1)$$

where,

$$G_I = -\frac{1}{2\Delta}\left[F_{ni}(v_k - v_{k'}) + F_{nj}(v_m - v_{m'})\right]$$

$$G_{II} = -\frac{1}{2\Delta}\left[F_{ti}(u_k - u_{k'}) + F_{nj}(u_m - u_{m'})\right]$$

and u and v are tangential and perpendicular nodal displacements respectively and F_t and F_n are the tangential and perpendicular nodal forces respectively

Delamination onset is assumed to occur when the calculated G exceeds the G_{crit} derived from material coupon delamination tests [8,13,15]. The details of estimating the probability of delamination onset are explained in the Section 5.2.2. A finite element model will be used to determine the local forces and displacements needed to calculate G as shown in Figure 4. The finite element model is discussed below.

5.1.4 *Structural model*

The geometry of the ANSYS finite element model for the problem is shown in Figure 5. The model consists of 6814 nodes and 2860 elements. The elements are of three types: 4-node quadrilateral, 8-node quadrilateral, and 6-node triangular elements. In the thick to taper transition region where delamination is critical, the finite element mesh is refined (see Figure 6) and modeled with 8-node quadrilateral elements. The average element size in this region is $1/4^{th}$ the ply thickness. Such small element size ensures that computation of the strain energy release rate, G, does not suffer from numerical inconsistencies. The resin pockets at the end of the dropped ply zones are modeled with 6-node triangular elements. The tension crack at the interface of the dropped ply zone and the resin pocket has been modeled with the help of contact elements. The delamination cracks at the interface of the belt plies and the dropped ply zones have been modeled with the help of duplicate multi point constraint (MPC) nodes.

5.1.5 *Calculation of laminate material properties*

A simple FORTRAN code has been written to compute the laminate material properties from the basic material properties. The method is well known, and is described in any textbook on composite materials mechanics, e.g., [18].

5.1.6 *ANSYS finite element stress analysis*

A nonlinear finite element analysis is executed for the stress analysis. The total load increment is divided into ten steps. In each step, a tenth of total loading is applied. The stiffness matrix is reassembled at each step and a maximum of 30 iterations is used for convergence of the stress analysis. A batch file in ANSYS is written to extract the displacements and the nodal forces at the elements around the delamination tip as a result of the stress analysis.

A program in C language is written to use the displacements and the nodal forces at the delamination tip to compute the strain energy release rate, G, according to the Eq. (4.1). The various steps in ANSYS stress analysis, including the building of the response surface model are illustrated in a flow chart in Figure 7.

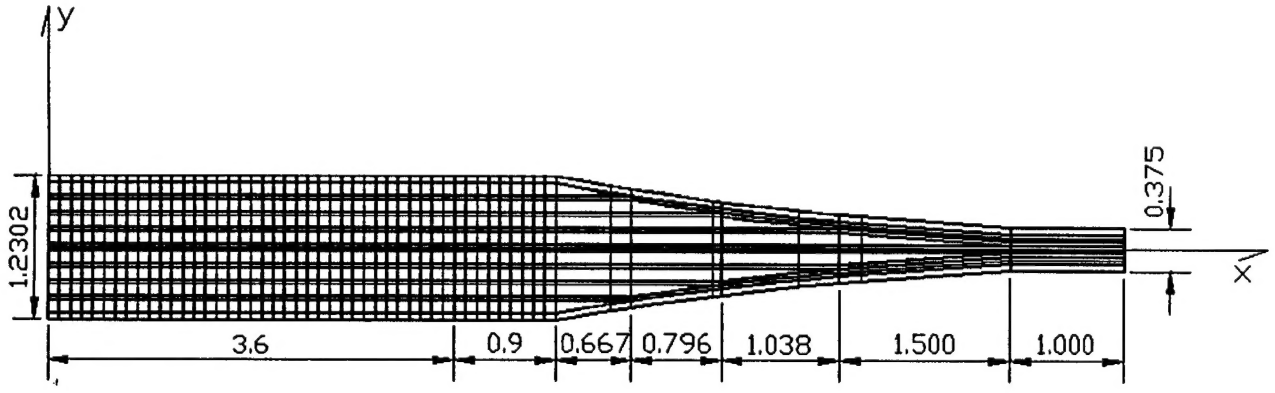

Figure 5: Model of tapered rotor hub

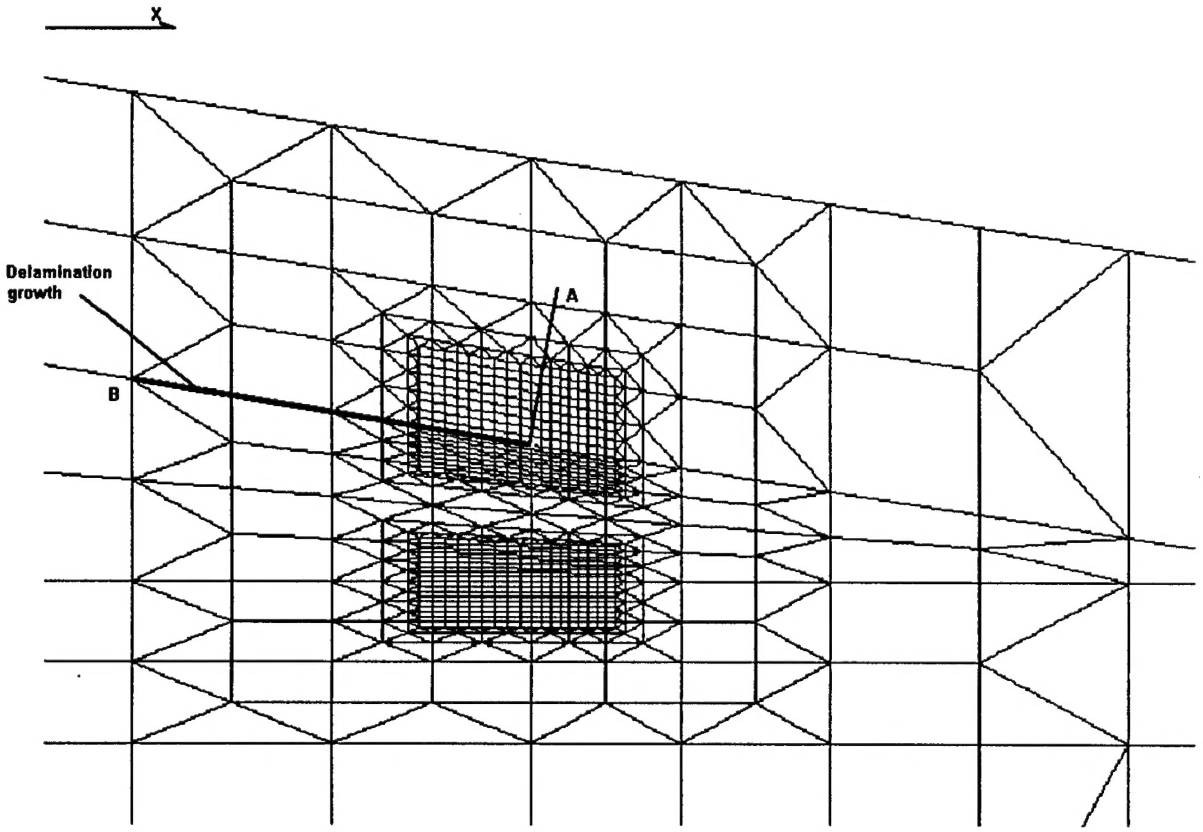

Figure 6 Refined mesh in the thick to taper transition.

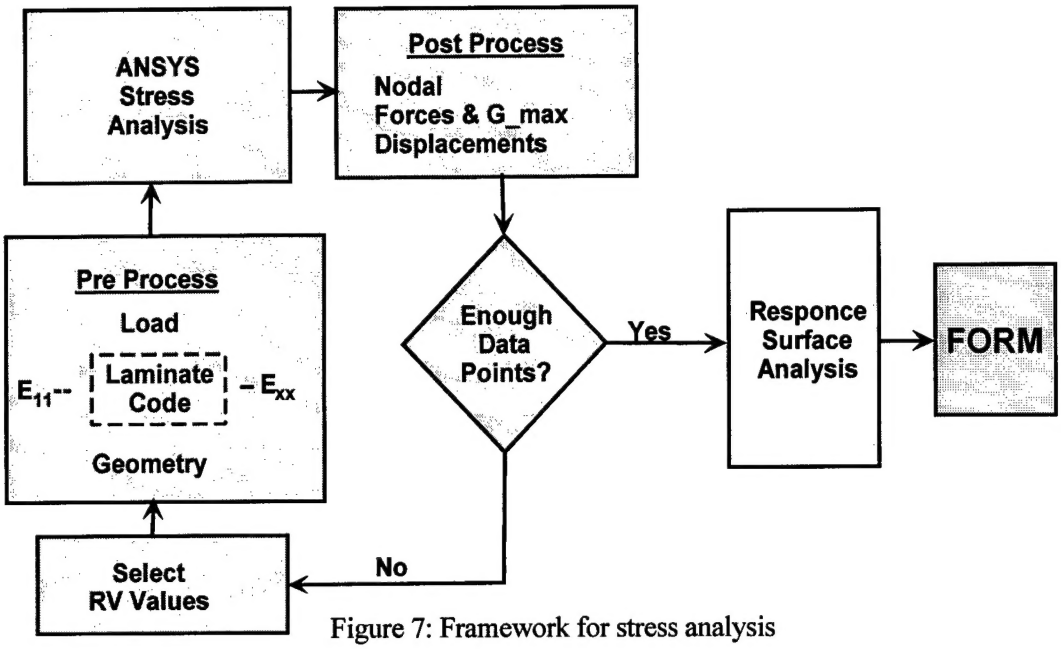

Figure 7: Framework for stress analysis

5.1.7 Delamination growth analysis

The objective of this task is to calculate the strain energy release rate for different delamination lengths and determine the delamination length at which the maximum strain energy release rate (G_{max}) is observed. Then the response surface method and direct FORM can be used to calculate the delamination probability of helicopter rotor.

Figure 6 shows the detail of delamination growth analysis: From point A to B, the duplicate nodes between elements along the delamination front are released step by step. In each step, nonlinear finite element analysis is performed and the G value at the delamination tip is calculated. Table 1 and Figure 8 show the relationship between the delamination length and the corresponding strain energy release rate. (Note: Delamination starts from X = 5.0, and grows to the left). The maximum G value of 1.014553 in-lb/in^2 is observed when the delamination length equals 0.026167 inch. The model with this delamination length is used further for response surface analysis as well as direct FORM analysis.

Table 1: G value and delamination length.

Delamination length (in)	0.016033	0.0211	0.026167	0.031234	0.036302	0.074312
G value (in-lb/in^2)	0.605323	0.891599	1.014553	0.944279	0.87124	0.447136
Delamination length (in)	0.114855	0.195935	0.25675	0.317564	0.378375	4.581083
G value (in-lb/in^2)	0.258372	0.17699	0.192102	0.237581	0.336777	0.459771

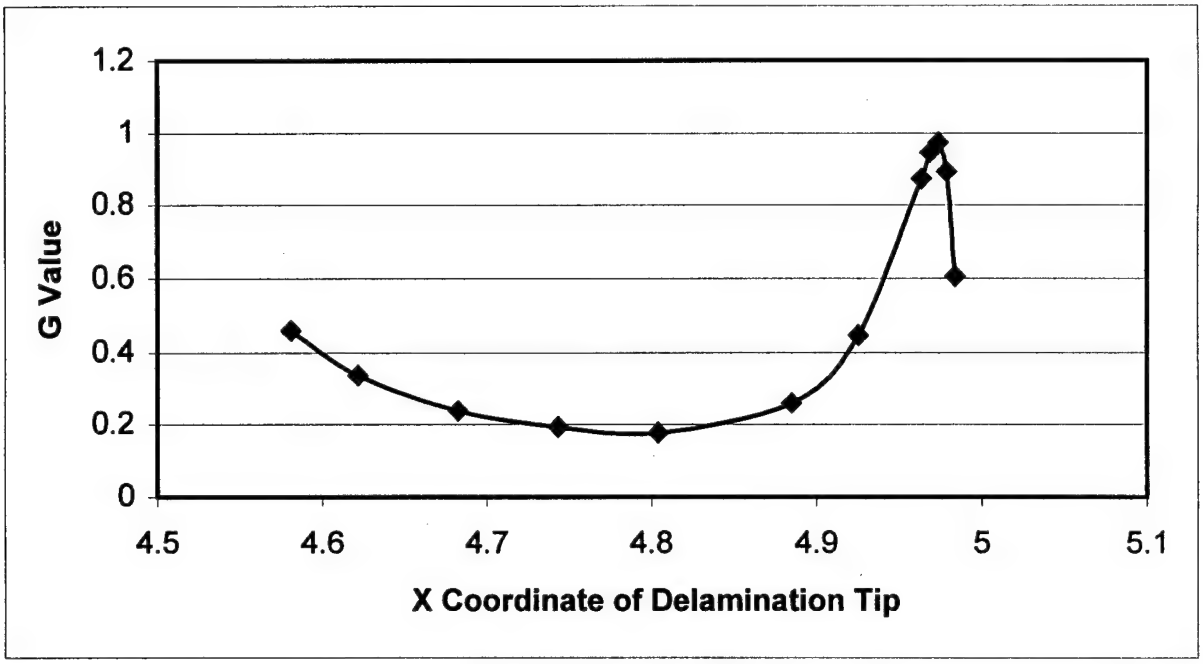

Figure 8: G values for different delamination lengths.

5.1.8 Random variable definition

Based on data from Bell Helicopter, seven random variables have been identified for probabilistic analysis with the finite element model of the helicopter rotor hub. These are material property variables E_{11}, E_{22}, ν_{13}, and G_{13}, the oscillatory bending angle θ caused by the cyclic loading, the magnitude of the axial load P, and the critical value of the strain energy release rate G_{crit}. All the random variables are assumed to be Gaussian (normal) for the purpose of demonstration, and their mean values and standard deviations are shown in Table 2.

Table 2 : Random variable description

S2/E7T1-2 Tape		
Property	Mean	Std. Deviation
E_{11} (Msi)	6.90	0.09
E_{22} (Msi)	1.83	0.05
G_{13} (Msi)	0.698	0.015
ν_{13}	0.28	0.01
P (kips)	30.8	3.08
θ (degrees)	12	1.67

The objective of the demonstration problem is to estimate the probability of initiation of delamination at the required life. This is assumed to occur when the strain energy release rate exceeds the limiting value G_{crit}, which is a function of load cycles, N. Figure 9 shows the G_{crit} *vs.* N as supplied by Bell Helicopter based on test data. Figure 9 also shows the best fit line through the data assuming G_{crit} is a linear function of $Log_{10}(N)$. According to Figure 9, the relationship between G_{crit} and N can be expressed as:

$$G_{crit} = 448.56 - 58.571 Log_{10}(N) \tag{4.2}$$

Based on statistical analysis of the G_{crit} *vs.* N data, it was determined that G_{crit} is a Gaussian (normal) random variable with its mean value described by Eq. (4.2) and a standard deviation of 36.6 J/m^2.

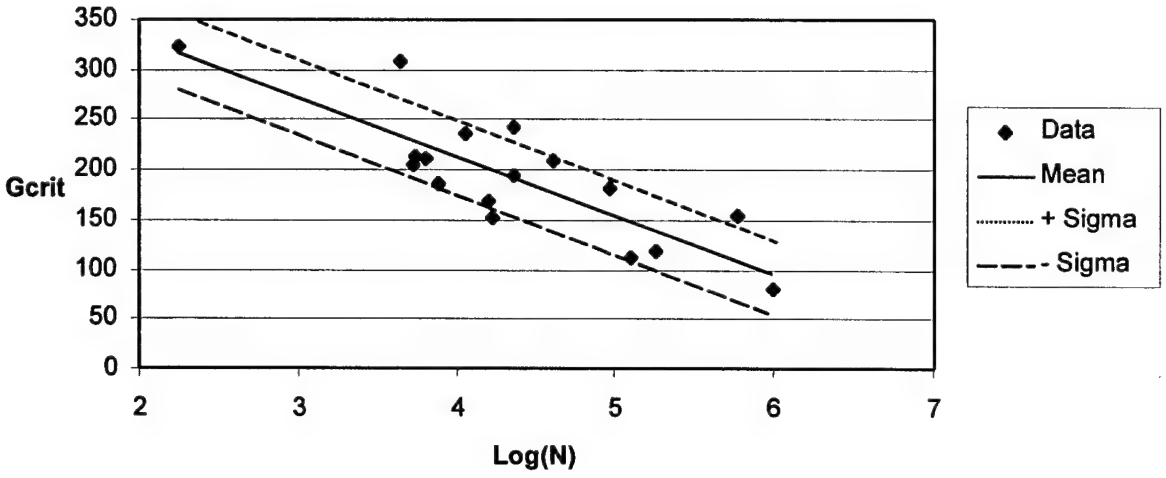

Figure 9: Relationship between G_crit and cycles of life.

5.2 Focus Area 2: Development of Reliability Analysis Module

This task requires developing a reliability analysis module using the First Order Reliability Method (FORM) [19]. The methodology of FORM requires describing the failure condition in a mathematical form as follows:

$$g = G_{crit} - G_{max} \tag{4.3}$$

Eq. (4.3) is called the limit state function. The limit state is a characteristic of the system component that can be observed, and is defined to represent the failure of the component to attain a required level of performance. According to Eq. (4.3), $g \leq 0$, i.e., G_{max} exceeds G_{crit}, represents failure and $g > 0$ represents the safe state of the system. The limit state function relates the system performance to primitive random design variables. In this case, G_{crit} and G_{max} are random variables that are dependent on primitive random variables such as material properties, geometric properties, loading conditions, etc. which have inherent scatter in their definition. G_{crit} can be considered to be the capacity of the system and G_{max} can be considered to be the demand on the system. FORM uses a constrained linear optimization technique to estimate the probability of $g \leq 0$.

The main benefit of using probabilistic reliability techniques such as FORM to predict product performance is that they enable the engineer to determine the sensitivity of the probability of failure to individual random variables. Specifically, if probabilistic methods are used, the sensitivity of the probability of failure to changes in random variable mean and variance can be found in closed form [19].

The utilization of probabilistic methods to estimate product performance and reliability has several benefits:

1. Design performance sensitivities to changes in mean, variance and truncation of variables can be estimated using closed-form relationships.
2. Individual and system level estimates of performance and reliability can be found simultaneously.
3. Product sensitivities to performance, reliability and cost can be linked and optimization methods can be employed to determine the optimal product configuration.

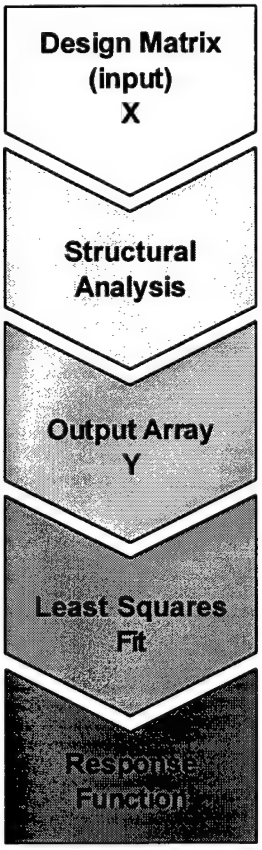

Figure 10: Response surface method.

5.2.1 Response surface modeling of the limit state

The limit state function in Eq. (4.3) is not available as a closed-form function of the basic random variables. It can only be computed through the ANSYS finite element stress analysis; thus it is an implicit function of the random variables. In such a case, the response surface approach, as shown in Figure 10, can be used to develop an approximate closed-form expression of the limit state function, and then the first-order reliability method (FORM) can be used to estimate the delamination probability. The response surface approach consists of two steps:

1. Design of experiments, i.e., the choice of different sets of values of the random variables to compute the corresponding values of the response g, and
2. Regression analysis, to construct the approximate closed-form function.

An initial regression analysis (screening analysis) including all seven random variables revealed that only three out of the seven random variables, namely, the bending angle (θ), magnitude of the axial load (P), and the material property E_{11}, had any significant effect on the limit state function. Therefore, for further analysis only three of the above mentioned random variables were included.

A Central Composite Design (CCD) (see Section 6.3) scheme was adopted to fit the response surface. For small number of random variables, such a design scheme is most efficient to explore the possibility of second-order effects and first order interaction terms among the random variables. A total of fifteen sets of experiments (non-linear finite element analyses) were performed to develop the response surface. The data sets for each experiment were gathered by selecting the value of each random variable at three levels, namely, mean, mean + 2 standard deviations and, mean- 2 standard deviations.

Table 3 shows the array of 15 experiments. A least squares regression of the data produced the equation:

$$G_{\max} = 1.006 + 8.402 \times 10^{-03} E_{11} + 0.138P + 0.191\theta + 5.432 \times 10^{-3} P^2 + 1.031 \times 10^{-2} \theta^2 + 2.359 \times 10^{-2} P\theta \quad (4.4)$$

As expected, the regression model (Eq.(4.4)) showed strong effect of the angle and magnitude of the load. Among the material property variables, E_{11} was also found to have some significance. Substituting Eq (4.4) into Eq (4.3) and maintaining consistency in units the final limit state equation is:

$$g = G_{crit} - 175.344(1.006 + 8.402 \times 10^{-03} E_{11} + 0.138P + 0.191\theta + 5.432 \times 10^{-3} P^2 + 1.031 \times 10^{-2} \theta^2 + 2.359 \times 10^{-2} P\theta) \quad (4.5)$$

Table 3: Response surface analysis data

No.	E_{11}(Msi)	P(Lb)	θ(Deg)	G_{max} (in-lb/in^2)
1	6.90	30800	12	1.014553
2	7.08	30800	12	0.998717
3	6.72	30800	12	1.031467
4	6.90	36960	12	1.273955
5	6.90	24640	12	0.668086
6	6.90	30800	15.333	1.434791
7	6.90	30800	8.667	0.633156
8	7.08	36960	15.333	1.766893
9	7.08	36960	8.667	0.817964
10	7.08	24640	15.333	0.99471
11	7.08	24640	8.667	0.468271
12	6.72	36960	15.333	1.774213
13	6.72	36960	8.667	0.832335
14	6.72	24640	15.333	1.09308
15	6.72	24640	8.667	0.483494

5.2.2 Reliability analysis

The objective of the Phase I research is to predict the probability of delamination onset in a helicopter rotor hub at a particular number of loading cycles. The steps involved in estimating the probability are:

1. Choose the number of loading cycles (N).
2. From Eq. (4.2) compute the mean value of G_{crit} associated with N.
3. With the limit state equation as defined in Eq. (4.5) , perform a FORM analysis to estimate the probability of delamination onset and the sensitivity of the random variables to the estimated probability.

Figure 11 shows the estimated probability of delamination onset at different values of the loading cycles. The mean predicted life is approximately 15000 cycles. Figure 12 shows the CDF plotted on lognormal paper. The linear form of the CDF in Figure 12 indicates that the fatigue life distribution is lognormal. The sensitivity results of the FORM analysis are shown in Table 4. It can be seen from the results that the bending angle θ, the axial load P, and G_{crit} are the most sensitive variables.

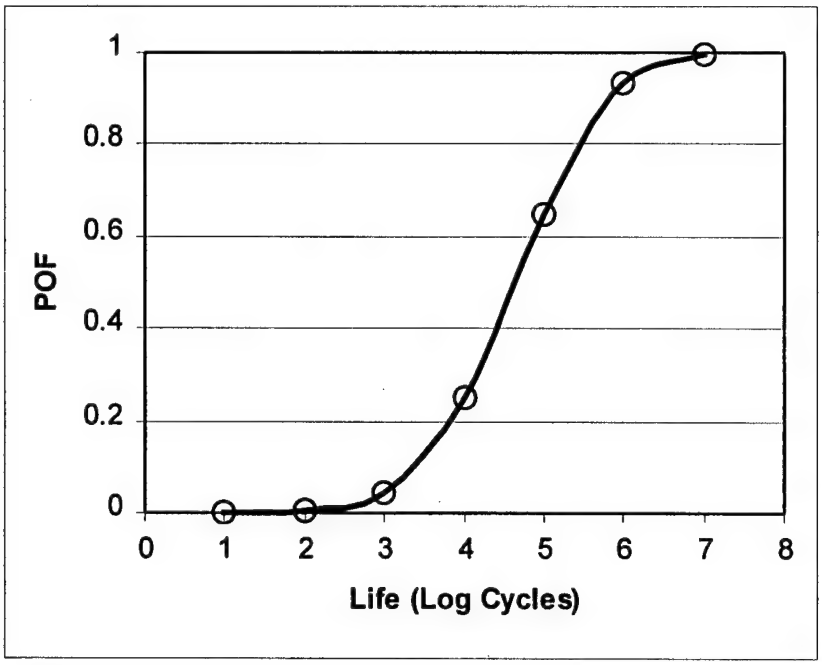

Figure 11: Cumulative distribution function (CDF) of delamination onset.

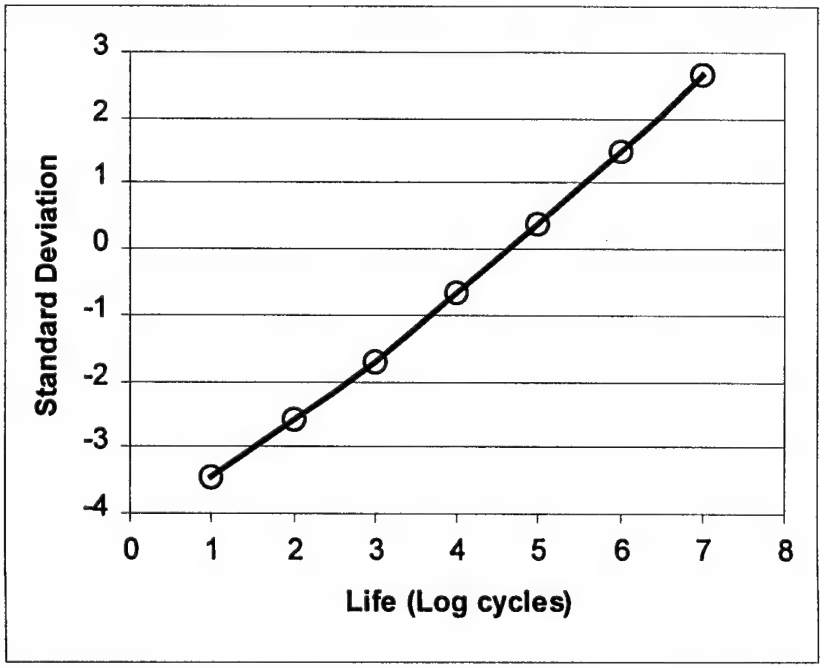

Figure 12: CDF plotted on lognormal paper

Table 4 :Sensitivity results

Log10(*N*)	G_{crit}	E_{11}	*P*	θ
1	-0.532	-0.0214	0.457	0.712
2	-0.564	-0.0227	0.452	0.690
3	-0.599	-0.0241	0.447	0.663
4	-0.637	-0.0256	0.442	0.631
5	-0.676	-0.0272	0.437	0.592
6	-0.713	-0.0287	0.436	0.548

5.3 Focus Area 3: Additional Reliability Algorithms

The composite design framework developed in the Phase I effort allow for two basic types of reliability analysis: response surface methods and mean value methods. The response surface method is best suited for the construction of the complete CDF. The complete CDF analysis is useful when the reliability is desired over a wide range of cyclic lives. For example, the designer may be interested in knowing the reliability for lives ranging from 1000 to 100,000 cycles. In this case, multiple finite element analyses are performed to create a global response surface that is approximate throughout the cyclic life range of interest. The response surface module includes a design of experiments routine to determine the matrix of input parameter values based on the desired fidelity of the response surface. The response surface method was used in the demonstration problem to determine the reliability of the tapered composite as discussed in Section 5. This section discusses the development of mean value-based reliability algorithms that have been added to the overall analysis framework.

Mean value methods restricts the finite element analyses to the region of the most probable failure point. This technique is useful when the reliability at a single value of life is of interest. For example, the designer may be interested in knowing the reliability only at a design requirement of 10,000 cycles. In this case, it is more efficient to perform multiple finite element analyses that are used to calculate the local response in the vicinity of 10,000 cycles. Two different routines were developed to perform the local reliability analysis; one based on Advanced Mean Value methods (AMV) and the other based on direct first order reliability techniques.

5.3.1 Mean value methods

Mean value methods are particularly suitable when a closed-form expression of the limit state is not directly available, as is the case when finite element analysis is used to model the structural response. The reliability computation algorithm developed for the Phase I effort constructs a linear approximation to the limit state in the equivalent standard normal space. Mean value methods works differently, as follows.

1. A first-order Taylor series approximation is constructed at the mean values of the random variables—in the *original space*—based on perturbation-based sensitivity analysis using the finite element analysis or other implicit response models. The two-parameter scheme is used to transform this closed-form approximation and the random variables to the equivalent standard normal space. The Rackwitz-Fiessler

iteration formula is used to estimate the MPP, and a first-order estimate of the failure probability is obtained similar to FORM. This is referred to as the mean value first-order (MVFO) estimate.

2. The MVFO estimate is refined using advanced mean value (AMV) analysis. This is simply a deterministic analysis of the system at the MPP, to evaluate the g-function. If the MVFO estimate were accurate, the g-function would be exactly zero. If the MVFO estimate were not accurate, then a different value would be obtained for the g-function. The MPP and the probability estimate identified by the MVFO are now assumed to correspond to this new value of the g-function.
3. The above two steps are repeated for different values of the g-function. This results in the construction of the CDF of the g-function.

Mean value methods are a practical alternative to FORM, if the deterministic analysis of the system is expensive. By simply combining the information from the MVFO step and one additional deterministic analysis, one is able to obtain a substantially improved estimate of the failure probability.

There are optimization algorithms, such as BEGS, which combine the information in the iteration steps to perform an accurate search. Such algorithms are especially useful when the Rackwitz-Fiessler algorithm fails to converge. However, the programming effort and the memory storage requirements in these methods, plus the marginal improvement in accuracy over the Rackwitz-Fiessler method have hindered their widespread application in structural reliability studies. The AMV, with its minimal one step combination, is a practical approach in this direction.

The AMV estimate can be further improved with more iteration. In the AMV + method, sensitivity analysis is performed after the AMV step, and steps 1 and 2 of the above procedure are repeated. In a similar manner, further iterations can be done to produce AMV + +, AMV + + +, etc., estimates. In each case, note that only the first iteration (MVFO) and the latest deterministic analysis are combined. It is important to note here that the sensitivity information in the AMV is computed only in the first iteration, i.e., at the MVFO step, which is at the mean values of the random variables. If the sensitivity values are needed at the MPP, then full sensitivity analysis needs to be performed.

The AMV method achieves accuracy through a quadratic approximation of the g function at the very beginning (at the mean values of the random variables). That is, the first-order derivatives can be calculated at the beginning using finite difference or perturbation analysis to have a second-order Taylor series approximation

$$g(X) \approx g(x^*) + \sum_{i=1}^{n} (x_i^*)_{x_i^*} (x_i - x_i^*) + \sum_{i=1}^{n} (2gpi)_{x_i^*} (x_i - x_i^*)^2 \times \sum_{i=1}^{n} a_i (x_i - x_i^*) + \sum_{i=1}^{n} b_i (x_i - x_i^*)^2 \quad (5.1)$$

Most reliability codes available today linearize the above expression. However, the use of a quadratic expression for the g function in Eq. (5.1) make the MPP and sensitivity estimates after the MVFO estimate more accurate. Notice, however, that the quadratic approximation of Eq. (5.1) does not involve mixed terms, and the effects of the random variables on the g-function are considered separately. This introduces some approximation.

5.3.2 MVFO/AMV software program

The MVFO and AMV methods described above were successfully transformed into a user-friendly computer program This section gives an example of how to use the method with the help of an example and screen dumps from the program. The mathematical details of the example are given in Section 6.2.3.

Example:

Assume we have a cantilever bean of length L, loaded at the free end with a force w. We wish to find the vertical displacement at the free end of the beam. We know that the load w, stiffness E, and the moment of inertia I, are all normally distributed random variables, with mean and standard deviation as follows:

$$w \approx N(5000,1000) \text{ lbs}$$

$$L \approx N(120,10) \text{ in}$$

$$E \approx N(30\times10^6,0.3\times10^6) \text{ psi}$$

$$I \approx N(1200,150) \text{ in}^4$$

We know from mechanics that the vertical displacement d of the free end of a beam is

$$d = \frac{wL^3}{3EI} \tag{5.2}$$

Let us assume, for this example, we could not determine the displacement in closed form and had to use a simple finite element model to determine the end displacement. The details of each step involved in performing a Mean Value First Order (MVFO) Analysis for the above example are enumerated below.

MVFO Analysis

Step 1. The first step is to input all of the above information into the computer program. Figure 13 and Figure 14 show the input screens for this step. It should be noted that random variables x1, x2, x3 and x4 refer to variables w, L, E and I respectively.

Step 2. The next step in a MVFO analysis is performing a perturbation analysis about the mean values of the input random variables (w, L, E, I) using the finite element model. The perturbation analysis is performed to determine the gradient $\frac{\partial z}{\partial x_i}$ of the response to each of the random variables. In this example z represents vertical tip displacement d, of the cantilever beam. The perturbation analysis involved changing each variable by one-tenth of its standard deviation about its mean value and rerunning the finite element model to create the array of five finite element runs as shown below. The results of the perturbation analysis are shown in Figure 15.

Step 3. Based on the perturbation analysis of Step 2, a first order Taylor Series expansion is performed about the mean values of the random variables expressing the vertical tip displacement d, as a function of the input variables. Figure 15 also shows this Taylor Series expansion expression.

Step 4. Having defined the Taylor Series expansion, the next step is to define the limit state equation for first order reliability analysis. The limit state equation is defined as:

$$g \equiv d_0 - d_{approx} \tag{5.3}$$

where d_0 is the "level of displacement" for which the reliability analysis is performed and d_{approx} is the Taylor Series expansion. In other words, the reliability analysis will find the probability that the beam displacement d_{approx} is greater than d_0. In the program d_0 is referred to as "Z-Level" (Figure 16). The user has a choice (a) either suggesting a range of Z-levels (d_0 values) based on a constant increment value (Automatic Z-Level Input) or (b) if the user is only interested in specific Z-levels, he/she can input those specific values individually (Manual Z-Level Input).

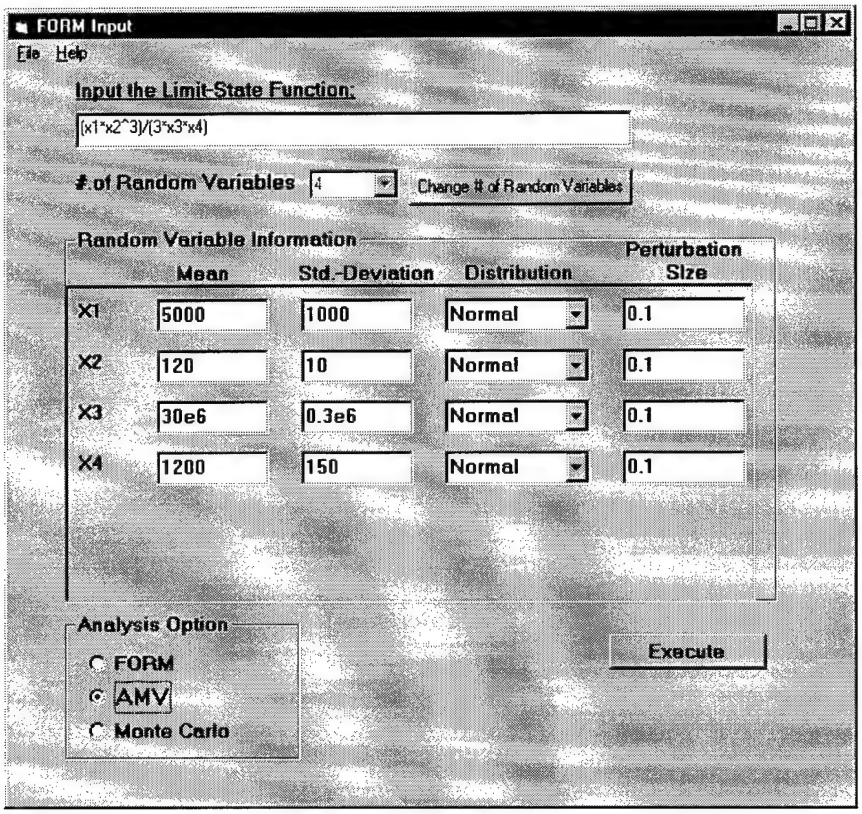

Figure 13: AMV input screen -1.

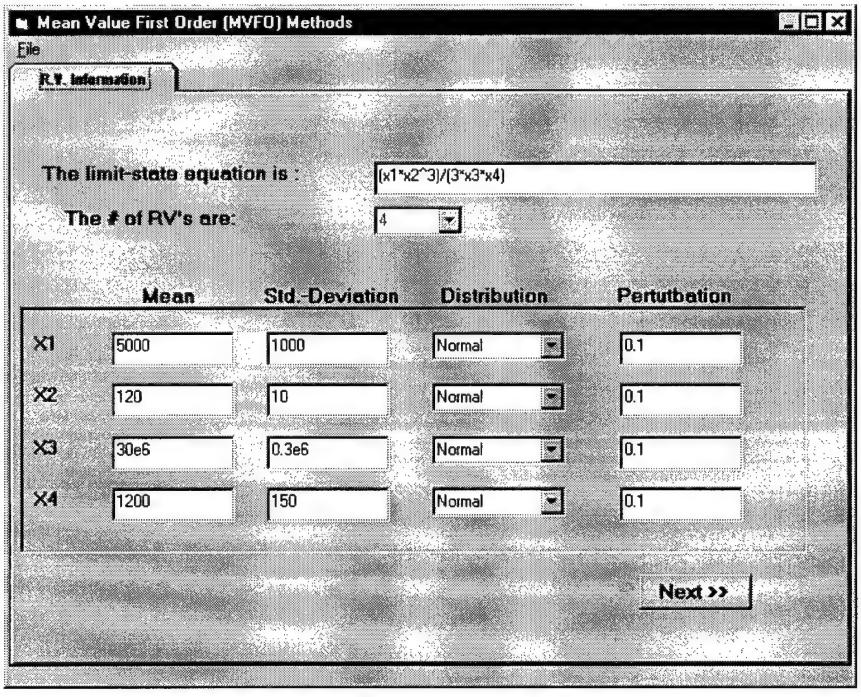

Figure 14: AMV input screen - 2.

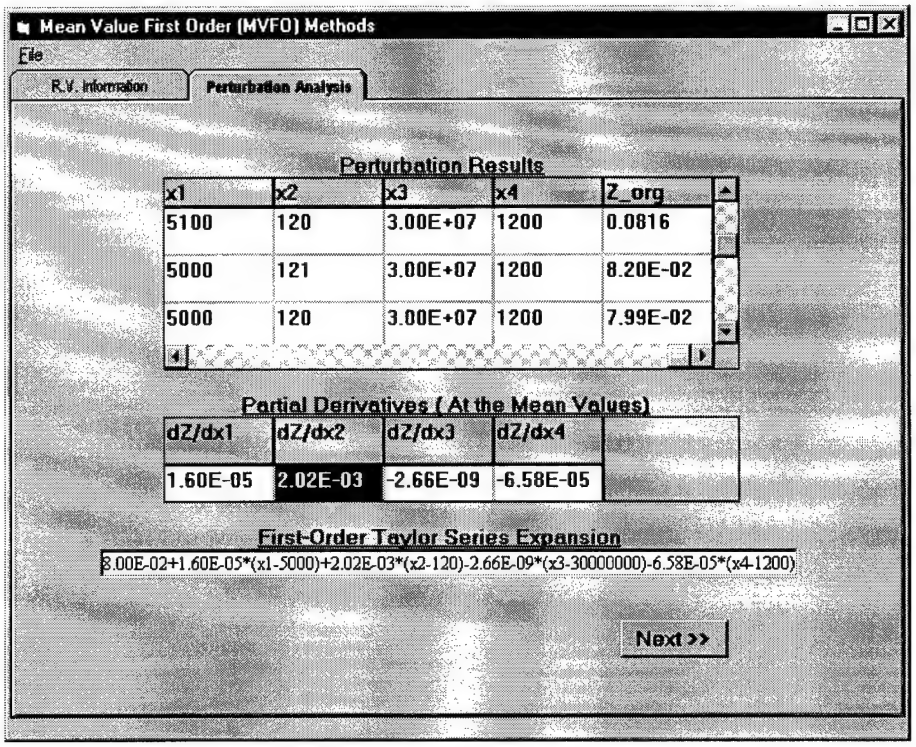

Figure 15: Perturbation analysis.

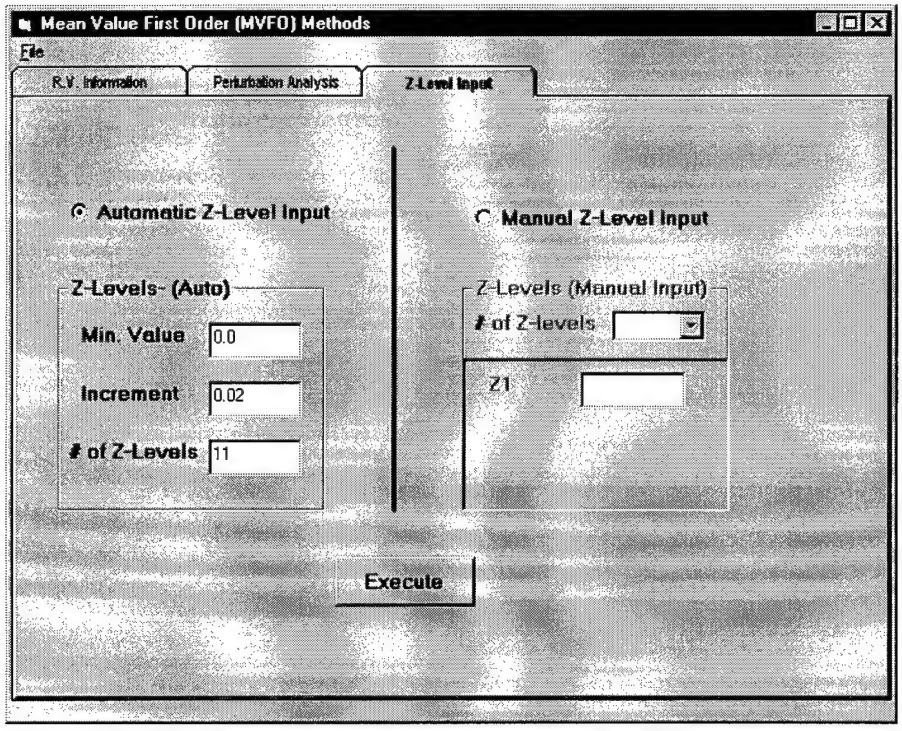

Figure 16: Z-level input.

Based on a range of values of d_0, the probability that $g \leq 0$ is determined. Figure 17 lists the range of values of d_0 considered along with the corresponding reliability indices (β) and the most probable values (MPP) of the input random variables (*w, L, E, I*) for which the relationship $g \leq 0$ was satisfied. Figure 17 also plots d_0 vs. β (z vs. beta) for the MVFO analysis, which represents the cumulative distribution function (CDF) of the vertical tip displacement *d* of the beam. Notice that the MVFO curve is linear. This is because the random variables are normal and a first-order approximation to the beam displacement response (equation (5.3)) was used in the analysis. However, we have no reason to believe that the true displacement response of the beam is linear. If we wish to develop a better approximation to the true CDF, we perform an advanced mean value analysis.

AMV Analysis

AMV is a continuation of the MVFO analysis in which we use the MPP from the MVFO analysis and the finite element model to further refine the reliability analysis.

Step 5. The vertical tip displacement based on the finite element analysis using the MPP values of the random variables is evaluated. These values are listed in the last column (z_org) of MVFO Results table in Figure 17. Notice that the value of the tip displacement from the finite element analysis (z_org) is not the same as d_0 (z-level). The value of d_0 (z-level) is equivalent to the value obtained by using Taylor Series approximation at the MPP. The displacement value at each β is shifted or "moved" from d_0 to d_{FEM} as show by the nonlinear AMV curve in Figure 17. The AMV curve is the CDF that represents a refinement to the MVFO CDF using just one additional finite element run.

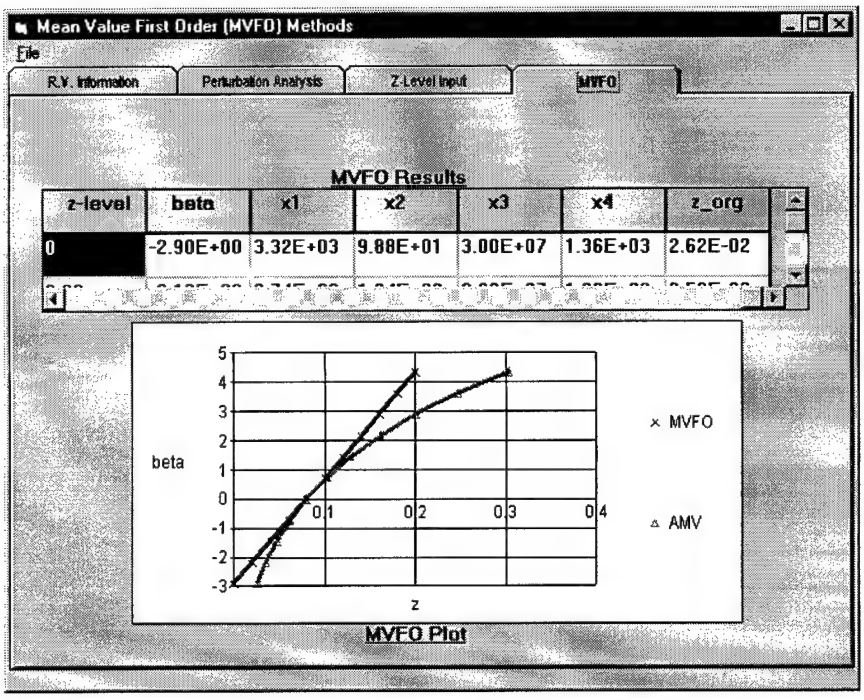

Figure 17: MVFO results.

5.3.3 *Direct FORM*

Direct FORM is an extension of the MVFO methods. In the direct FORM method, we do not construct a closed-form approximation to the limit state. The finite element analysis is used to compute the value and the gradient of the limit state at each iteration of FORM is used to search for the most probable point (MPP). The number of iterations is based on the convergence of β and the MPP. Thus, AMV can be considered a subset of direct FORM.

To implement the direct FORM method, a C program has been written to directly integrate finite element analysis and reliability analysis. The program does the following steps:

1. Read the mean value and standard deviation of each random variable as input data.
2. Call the laminate code to calculate the material properties of laminate model.
3. Generate the input file for calling the finite element software as a subroutine to perform the structural analysis of the rotor hub component.
4. Read the finite element analysis output file and calculate the limit state function $g(x)$ and its derivatives with respect to the random variables.
5. Use FORM to compute the next iteration point in the search for the MPP.

Steps 2 to 5 are repeated at each iteration until the program converges to the MPP. This provides the estimate of the reliability index β and the delamination probability of rotor hub component.

The direct FORM program is re-run for different number of cycles of fatigue life, and the probability of failure vs. number of cycles is computed. For this problem, the results of direct FORM are observed to be within 10% of the results with the response surface approach.

6 Theoretical Background for Reliability-Based Design

6.1 Interference Theory

Reliability-based design stems from the concepts of interference theory. Interference theory is used to find the probability that the resistance (r) of a component or system is less that the applied load (l). The simple mathematical function that describes the performance of the design is

$$g = r - l \qquad (6.1)$$

which is called the *response* or *performance* function. The regime in which $g = r - l > 0$ is the safe state, the regime in which $g = r - l < 0$ is the failure state, and the state $g = r - l = 0$ separates the safe state from the failure state and is called the *limit*-state.

The term interference theory comes from the graphical representation of the *PDF* for the resistance and load as shown show in Figure 18. The failure state can be associated with the shaded region. This region is associated with the probability of failure or the probability that the resistance is less than the load,

$$P(\hat{r} < \hat{l}) = P(\hat{r} - \hat{l} < 0) = P(\hat{g} < 0)$$

which is the probability that the resistance random variable $\hat{r}$ is less than a realization of the load l multiplied by the probability that the load random variable $\hat{l}$ is equal to the realization l for all realizations of the load,

$$P(\hat{r} < \hat{l}) = \sum_{\text{all } l} P(\hat{r} < l) P(\hat{l} < l) \qquad (6.2)$$

We know that the probability that $\hat{r}$ is less than l is equal to the *CDF* of r at l.

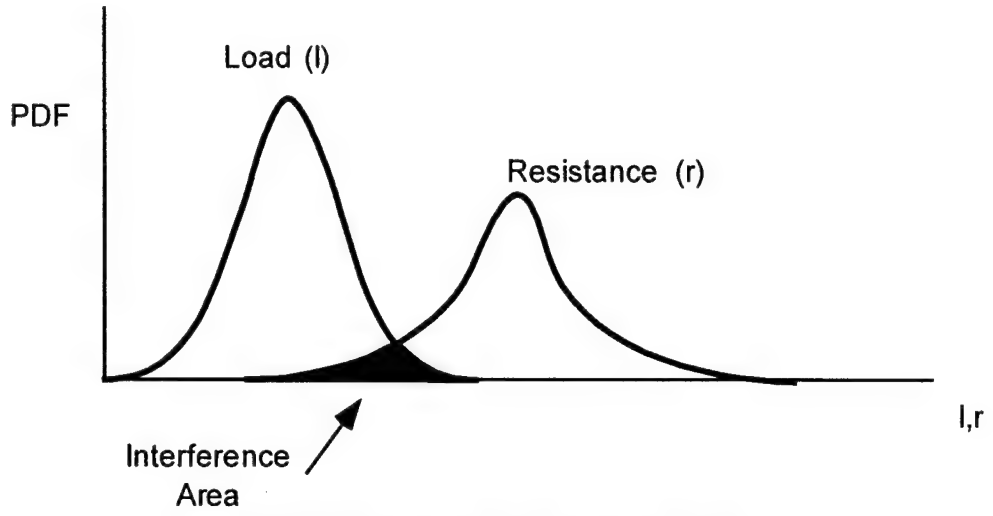

Figure 18: Resistance load interference diagram.

$$P(\hat{r} < l) = F_r(l) \qquad (6.3)$$

and the probability that $\hat{l}$ is equal to l is the probability that $\hat{l}$ is between l and a small increment Δl.

$$P(\hat{l} < l) = P(l < \hat{l} < l + \Delta l)$$
$$P(\hat{l} < l) = f_l(l)\Delta l \qquad (6.4)$$

Substituting (6.3) and (6.4) into (6.2) yields

$$P(\hat{r} < \hat{l}) = \sum_{\text{all } l} F_r(l) f_l(l) \Delta l \qquad (6.5)$$

The expressions in (6.5) are represented graphically in Figure 19.

As Δl becomes infinitesimally small and approaches dl, the probability of failure can be expressed as

$$P(\hat{r} < \hat{l}) = \int_0^\infty F_r(l) f_l(l) dl \qquad (6.6)$$

Alternatively, we can consider the probability of failure as the probability that the load is greater than the resistance

$$P(\hat{l} > \hat{r}) = \int_0^\infty [1 - F_l(r)] f_r(r) dr \qquad (6.7)$$

For particular statistical distributions of resistance and load, direct solutions to (6.6) (or (6.7)) are available [Kapur and Lamberson, 1977]. If $\hat{r}$ and $\hat{l}$ are independent normal (Gaussian) random variables, then

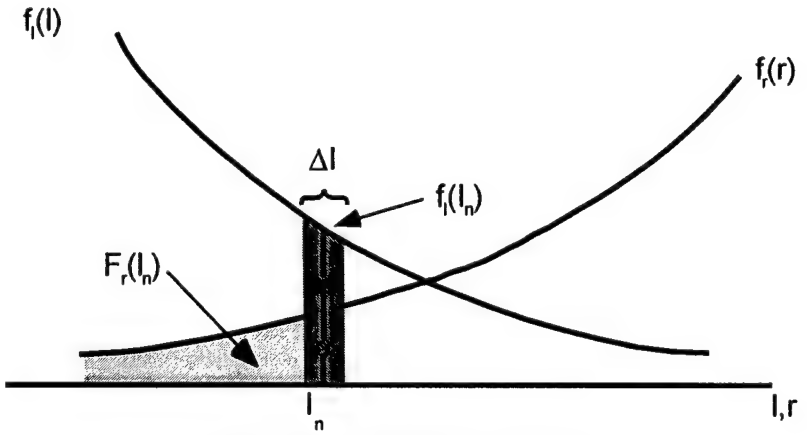

Figure 19: Interference diagram.

$$\hat{r} \sim N(\mu_r, \sigma_r)$$
$$\hat{l} \sim N(\mu_l, \sigma_l) \qquad (6.8)$$

$$\int_0^\infty F_r(l) f_l(l) dl = \Phi(-\beta) \qquad (6.9)$$

$$\beta = \frac{\mu_r - \mu_l}{\sqrt{\sigma_r^2 + \sigma_l^2}} \qquad (6.10)$$

where Φ is the standard normal *CDF* and β is referred to as the *reliability index* or *safety index*.

Recall that for linear functions of independent random variables, the mean value of the function is equal to the function evaluated at the mean values of the individual variables and therefore the mean value of $g = r - l$ is

$$\mu_g = \mu_r - \mu_l$$

and the variance of g is the square root of the sum of the squares of the variance of the individual random variables

$$\sigma_g = \sqrt{\sigma_r^2 + \sigma_l^2}$$

The safety index (6.10) can be written as

$$\beta = \frac{\mu_r - \mu_l}{\sqrt{\sigma_r^2 + \sigma_l^2}} = \frac{\mu_g}{\sigma_g} \qquad (6.11)$$

which is the inverse of the COV of g.

If $\hat{r}$ and $\hat{l}$ are independent lognormal random variables, then

$$\hat{r} \sim LN(E(\hat{r}), StdDev(\hat{r}))$$
$$l \sim LN(E(\hat{l}), StdDev(\hat{l}))$$
$$\sigma_x^2 = \ln\left[\frac{StdDev(\hat{x})^2}{E(\hat{x})^2} + 1\right]$$
$$\mu_x = \ln E(\hat{x}) - \frac{1}{2}\sigma_x^2$$
$$\int_0^\infty F_r(l) f_l(l) dl = \Phi(-\beta)$$
$$\beta = \frac{\mu_r - \mu_l}{\sqrt{\sigma_r^2 + \sigma_l^2}} \qquad (6.12)$$

where $E(\hat{x})$ is the expected value and $StdDev(\hat{x})$ is the standard deviation. If $\hat{r}$ and $\hat{l}$ are independent exponential random variables, then

$$E(\hat{r}) = \frac{1}{\lambda_r}$$
$$E(\hat{l}) = \frac{1}{\lambda_l}$$
$$\int_0^\infty F_r(l) f_l(l) dl = 1 - \frac{\lambda_l}{\lambda_r - \lambda_l} = \frac{E(\hat{r})}{E(\hat{r}) + E(\hat{l})} \qquad (6.13)$$

If $\hat{r}$ and $\hat{l}$ are independent and $\hat{r}$ is normal and $\hat{l}$ is exponential, then

$$\hat{r} \sim N(\mu_r, \sigma_r)$$
$$\hat{l} \sim EXPO(\lambda_l)$$

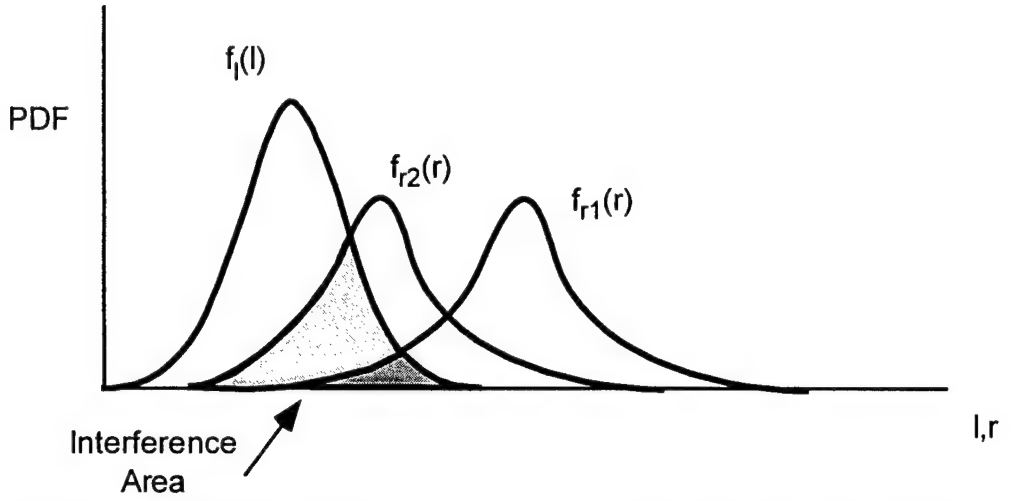

Figure 20: Interference diagram showing increase in interference area with decrease in safety measures.

$$\int_0^\infty F_r(l) f_l(l) dl = \Phi\left(-\frac{\mu_r}{\sigma_r}\right) - \exp\left[-\frac{1}{2}\left(2\mu_r\lambda_l - \lambda_l^2\sigma_r^2\right)\right]\left[1 - \Phi\left(-\frac{\mu_r - \lambda_l^2\sigma_r^2}{\sigma_r}\right)\right] \qquad (6.14)$$

If $\hat{r}$ and $\hat{l}$ are independent and $\hat{r}$ is exponential and $\hat{l}$ is normal, then

$$\hat{r} \sim EXPO(\lambda_r)$$

$$\hat{l} \sim N(\mu_l, \sigma_l)$$

$$\int_0^\infty F_r(l) f_l(l) dl = 1 - \Phi\left(-\frac{\mu_l}{\sigma_l}\right) + \exp\left[-\frac{1}{2}\left(2\mu_l\lambda_r - \lambda_r^2\sigma_l^2\right)\right]\left[1 - \Phi\left(-\frac{\mu_l - \lambda_r^2\sigma_l^2}{\sigma_l}\right)\right] \qquad (6.15)$$

The probability of failure depends on the mean (or average) value of the resistance and load. As the difference between the mean resistance and mean load increases, the probability of failure decreases. If the difference between the mean resistance and mean load decreases, the probability of failure increases. This is shown graphically in Figure 20. Note that the ratio of the mean resistance to the mean load is equivalent to the safety factor used in deterministic analysis.

$$\text{safety factor} = \left(\frac{\mu_r}{\mu_l}\right) \qquad (6.16)$$

The difference between the mean resistance and the mean load is the safety margin used in deterministic analysis.

$$\text{safety margin} = \mu_r - \mu_l \qquad (6.17)$$

As the safety factor or safety margin decrease, the probability of failure increases.

The probability of failure also depends on the scatter or degree or dispersion of the resistance and load. If either the scatter in resistance or the scatter in load increases, the probability of failure increases. Figure 21 shows that as the scatter increases, the size of the interference region increase. The change in probability of failure with changes in the mean values and scatter of the random variables can also be observed by considering the magnitude of the safety index β as shown in (6.10).

We have shown two methods for decreasing the probability of failure of a design. One method is to increase the relative distance between the mean resistance and the mean load. This is the result of traditional design improvements which is equivalent to increasing the safety factor. The other method, which traditional design improvement does not address, is to decrease the scatter in the resistance and/or load variables.

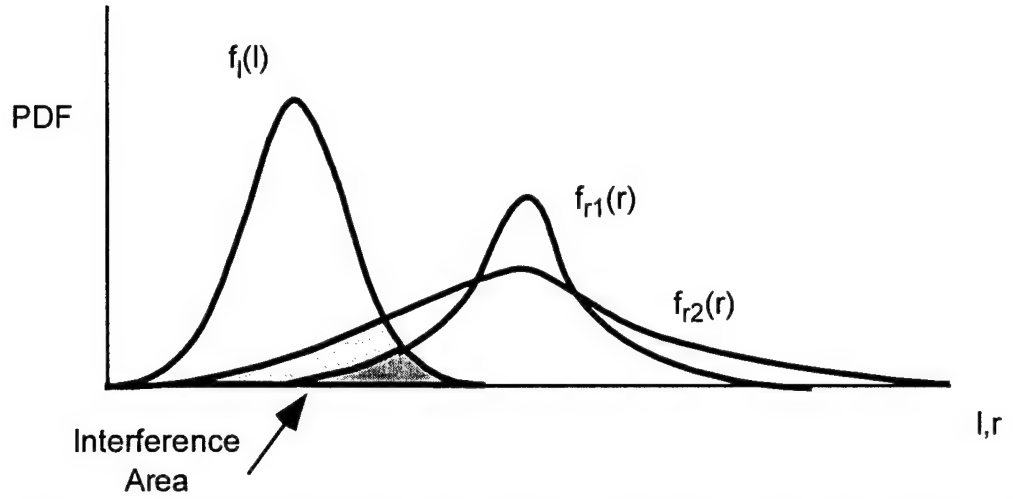

Figure 21: Interference diagram showing increase in interference area with increase in scatter.

Addressing the scatter in the design parameters gives the design a whole different method to improve the reliability, efficiency, and competitiveness of a design. Increasing the safety factor has been the most popular design improvement method because methods addressing scatter have not been widely available except for the simple $r-l$ performance function and a limited variety of statistical distributions. Tabulated numerical solutions to (6.6) for other distribution type (most notably Weibull) are available (see Kapur and Lamberson, 1977). However, these solutions are still based on the simple $r-l$ performance function.

Let us consider a simple yet realistic design of a cantilever beam. Assume the beam is subjected to a point load w at the free end. The design criteria specifies that the displacement d at the free end does not exceed the a specific value denoted by z. From mechanics of materials, we know a performance function describing the end displacement is

$$d = \frac{wL^3}{3EI} \qquad (6.18)$$

where w is the load, L is the length of the beam, E is Young's modulus of the beam material, and I is the cross sectional moment of the beam. The limit state that separates the safe region from the failure region is

$$g = z - d = z - \frac{wL^3}{3EI} = 0 \quad (6.19)$$

Assume the deflection criteria z is deterministic and the load, length, modulus, and moment are all random variables with the following distributions:

$$\hat{w} \sim N(\mu_w, \sigma_w)$$
$$\hat{L} \sim LN(\lambda_L, \zeta_L)$$
$$\hat{I} \sim LN(\lambda_I, \zeta_I)$$
$$\hat{E} \sim WB(b_E, \eta_E, \gamma_E)$$

The probability of failure is formulated as

$$P_f = P\left(z < \frac{\hat{w}\hat{L}^3}{3\hat{E}\hat{I}}\right) \qquad (6.20)$$

We rewrite (6.20) so that we have random variables on both sides of the inequality

$$P_f = P\left(\hat{w} > \frac{3z\hat{E}\hat{I}}{\hat{L}^3}\right) \qquad (6.21)$$

We know from (6.7) that

$$P\left(\hat{w} > \frac{3z\hat{E}\hat{I}}{\hat{L}^3}\right) = \int_0^\infty\int_0^\infty\int_0^\infty \left[1 - F_{\hat{w}}\left(\frac{3zEI}{L^3}\right)\right] f_{\hat{L}}(L) f_{\hat{I}}(I) f_{\hat{E}}(E)\, dL\, dI\, dE \qquad (6.22)$$

The distribution functions are defined as

$$F_{\hat{w}}\left(\frac{3zEI}{L^3}\right) = \frac{1}{\sigma_w\sqrt{2\pi}} \int_0^{\frac{3zEI}{L^3}} \exp\left[-\frac{1}{2}\left(\frac{x-\mu_w}{\sigma_w}\right)^2\right] dx \text{ (Gaussian)} \qquad (6.23)$$

$$f_{\hat{L}}(L) = \frac{1}{\sqrt{2\pi}\zeta_L L} \exp\left[-\frac{1}{2}\left(\frac{\ln L - \lambda_L}{\zeta_L}\right)\right] \text{ (lognormal)} \qquad (6.24)$$

$$f_{\hat{I}}(I) = \frac{1}{\sqrt{2\pi}\zeta_I I} \exp\left[-\frac{1}{2}\left(\frac{\ln I - \lambda_I}{\zeta_I}\right)\right] \text{ (lognormal)} \qquad (6.25)$$

$$f_{\hat{E}}(E) = \frac{b_E}{\eta_E}\left(\frac{E-\gamma_E}{\eta_E}\right)^{b_E-1} \exp\left[-\left(\frac{E-\gamma_E}{\eta_E}\right)^{b_E}\right] \text{ (Weibull)} \qquad (6.26)$$

Although the performance function describing the displacement of the beam (6.18) is simple, substituting (6.23) through (6.26) into (6.22) creates a multiple integral that is difficult, if not impossible to solve. Using direct integration to find the probability of failure for most engineering designs is not practical.

6.2 Second Moment Formulation

Due to the impracticality of solving the multiple integral associated with the interference region, second moment formulations have been developed to approximate the probability of failure. The term second moment formulation refers to the transformation of the random variable statistics into equivalent standard normal variables described only by the first and second moments, μ and σ respectively. We will develop the second moment formulation based on the simple $r - l$ performance function with both $\hat{r}$ and $\hat{l}$ as independent Gaussian random variables. The formulation will then be generalized for more complicated performance functions and various types of statistical distributions.

6.2.1 Linear response functions

If $g = r - l$ then we observe that

$$(g > 0) \rightarrow (r > l) \text{ is the safe state}$$
$$(g < 0) \rightarrow (r < l) \text{ is the failure state}$$
$$(g = 0) \rightarrow (r = l) \text{ is the limit state}$$

If we transform $\hat{r} \rightarrow N(\mu_r, \sigma_r)$ and $\hat{l} \rightarrow N(\mu_l, \sigma_l)$ into standard normal variables $\hat{r}' \rightarrow N(1,0)$ and $\hat{l}' \rightarrow N(1,0)$

$$\hat{r}' = \frac{\hat{r} - \mu_r}{\sigma_r} \rightarrow \hat{r} = \sigma_r \hat{r}' + \mu_r \qquad (6.27)$$

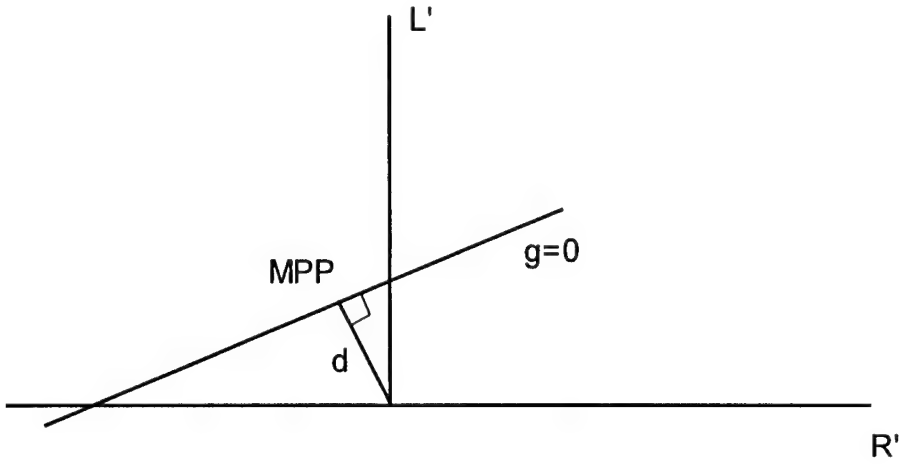

Figure 22: Linear limit state equation in standard normal space.

$$\hat{l}' = \frac{\hat{l} - \mu_l}{\sigma_l} \rightarrow \hat{l} = \sigma_l \hat{l}' + \mu_l \qquad (6.28)$$

The limit state equation can now be written as

$$g = 0 = \hat{r} - \hat{l} = \sigma_r \hat{r}' + \mu_r - \sigma_l \hat{l}' - \mu_l \qquad (6.29)$$

If we plot (6.29) in standard normal space (considering the (r', l') axis), we get a straight line as shown in Figure 22.

We know that the minimum (perpendicular) distance δ of any line

$$ax + by + c = 0 \quad (6.30)$$

to the origin is

$$\delta = \frac{c}{\sqrt{a^2 + b^2}} \quad (6.31)$$

If we put (6.29) in the form of (6.30)

$$g = (\sigma_r)\hat{r}' + (-\sigma_l)\hat{l}' + (\mu_r - \mu_l) = 0 \qquad (6.32)$$

then the minimum distance δ to the origin is

$$\delta = \frac{\mu_r - \mu_l}{\sqrt{\sigma_r^2 + \sigma_l^2}} \quad (6.33)$$

Comparing (6.33) to (6.10) we notice that δ is equal to the safety index β and thus the probability of failure for the performance function is

$$P_f = \Phi(-\delta) \qquad (6.34)$$

The point on the limit state line which is closest to the origin is called the *most probable point* (MPP) designated $(\hat{r}'^{\bullet}, \hat{l}'^{\bullet})$. Of all of the values of $(\hat{r}', \hat{l}')$ which cause failure, the MPP value can be thought of, in some approximate sense, as the value of $(\hat{r}', \hat{l}')$ which are most likely to occur. The MPP is an important concept in the second moment formulation because the distance from the MPP to the origin is the safety index. Also, approximation methods that allow us to consider complex performance functions must make use of the MPP.

The $x_i'^*$ coordinate of the MPP can be found using analytical geometry

$$x_i'^* = -\alpha_i^* \beta \qquad (6.35)$$

where α_i^* is the cosine of the angle between the β vector and the X_i' axis

$$\alpha_i^* = \frac{\dfrac{\partial g}{\partial x_i'}}{\sqrt{\sum_{i=1}^{n}\left(\dfrac{\partial g}{\partial x_i'}\right)^2}} \qquad (6.36)$$

(We will drive (6.36) later.) If we apply the above formulations to the simple linear performance function $g = r - l$ with both $\hat{r}$ and $\hat{l}$ as independent Gaussian random variables, the limit state function transformed into standard normal variables $\left(\hat{r}', \hat{l}'\right)$ is

$$g = (\sigma_r)\hat{r}' + (-\sigma_l)\hat{l}' + (\mu_r - \mu_l) = 0 \qquad (6.37)$$

with safety index

$$\beta = \frac{\mu_r - \mu_l}{\sqrt{\sigma_r^2 + \sigma_l^2}}$$

The MPP in standard normal space is designated $\left(r'^*, l'^*\right)$ where

$$\left(r'^*, l'^*\right) = \left(-\alpha_r^* \beta, -\alpha_l^* \beta\right)$$

$$\alpha_r^* = \frac{\dfrac{\partial g}{\partial \hat{r}'}}{\sqrt{\left(\dfrac{\partial g}{\partial \hat{r}'}\right)^2 + \left(\dfrac{\partial g}{\partial \hat{l}'}\right)^2}}$$

$$\alpha_l^* = \frac{\dfrac{\partial g}{\partial \hat{l}'}}{\sqrt{\left(\dfrac{\partial g}{\partial \hat{r}'}\right)^2 + \left(\dfrac{\partial g}{\partial \hat{l}'}\right)^2}}$$

Differentiating (6.37) with respect to $\hat{r}'$ and $\hat{l}'$ respectively

$$\frac{\partial g}{\partial \hat{r}'} = \sigma_r$$

$$\frac{\partial g}{\partial \hat{l}'} = \sigma_l$$

Therefore,

$$\alpha_r^* = \frac{\sigma_r}{\sqrt{\sigma_r^2 + \sigma_l^2}}$$

$$\alpha_l^* = \frac{-\sigma_l}{\sqrt{\sigma_r^2 + \sigma_l^2}}$$

and the MPP in standard normal space is

$$\left(r'^*, l'^*\right) = \left(\frac{-\sigma_r \beta}{\sqrt{\sigma_r^2 + \sigma_l^2}}, \frac{\sigma_l \beta}{\sqrt{\sigma_r^2 + \sigma_l^2}}\right)$$

The direction cosines α_i^* are also called the *variable importance factors* (VIF). They provide a relative measure of the sensitivity of the reliability to the random variable X_i. The sign of α_i^* indicates the influence of the variable on the reliability. The positive sign on α_r^* indicates that as the resistance increases, the reliability increases. The negative sign on α_l^* indicates that as the load increases, the reliability decreases.

The MPP in real space is

$$\left(r^*, l^*\right) = \left(\frac{\frac{-\sigma_r \beta}{\sqrt{\sigma_r^2 + \sigma_l^2}} - \mu_r}{\sigma_r}, \frac{\frac{\sigma_l \beta}{\sqrt{\sigma_r^2 + \sigma_l^2}} - \mu_l}{\sigma_l} \right)$$

Numerical Example 6.1: Assume we are interested in analyzing an automatic assembly process in which 3 steel sheets are stacked on top or each other and inserted into a plastic clip as shown in Figure 23.

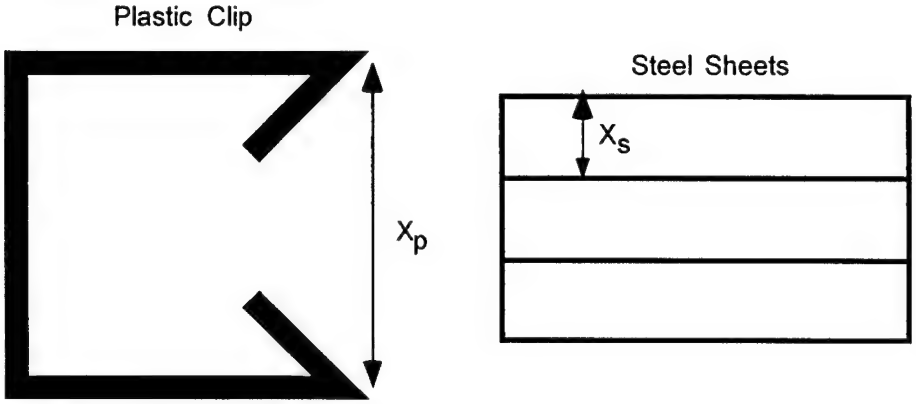

Figure 23: Steel sheets insert into the plastic clip.

The assembly process fails when the stack of steel sheets is too thick to fit into the plastic clip. The performance function is defined as

$$g = x_p - 3x_s \qquad (6.38)$$

We define the probability of failure as the probability that the clip opening is less than the stack thickness.

$$P_f = P\left(x_p < 3x_s\right) \qquad (6.39)$$

The limit state equation associated with the (6.38) is

$$g = 0 = x_p - 3x_s \qquad (6.40)$$

We know that measurements made during statistical process control indicate that the sheet thickness and the clip opening have the following statistical distributions:

$$x_s \sim N(\mu_s, \sigma_s) = N(1 \text{ in}, 0.1 \text{ in})$$

$$x_p \sim N(\mu_p, \sigma_p) = N(4 \text{ in}, 0.8 \text{ in})$$

The steel sheets and the plastic clips are manufactured by completely different methods. So, it is fair to assume that the sheet thickness and the clip opening are independent random variables.

To find the probability of failure we transform the random variables (x_s, x_p) into standard normal variables

$$\hat{x}_s' = \frac{\hat{x}_s - \mu_s}{\sigma_s} \Rightarrow \hat{x}_s = \sigma_s \hat{x}_s' + \mu_s$$
$$\hat{x}_p' = \frac{\hat{x}_p - \mu_p}{\sigma_p} \Rightarrow \hat{x}_p = \sigma_p \hat{x}_p' + \mu_p \qquad (6.41)$$

Substituting (6.41) into (6.38) yields

$$g = 0 = (\sigma_p)\hat{x}_p' + (-3\sigma_s)\hat{x}_s' + (\mu_p - 3\mu_s) \qquad (6.42)$$

Comparing (6.42) to (6.32) allow us to solve for the safety index β, which is the minimum distance from the line $g = 0$ to the origin as in (6.33).

$$\beta = \frac{\mu_p - 3\mu_s}{\sqrt{\sigma_p^2 + (3\sigma_s)^2}} = \frac{4-3}{\sqrt{0.8^2 - 0.3^2}} = 1.17$$

The probability of failure is

$$P_f = \Phi(-\beta) = \Phi(-1.17) = 0.121$$

Which indicates that about 12% of the assemblies will fail.

It is interesting to note that the deterministic analysis tell us that we have a safety margin of 1 inch and a safety factor of

$$\text{safety factor} = \frac{\mu_p}{3\mu_s} = \frac{4}{3} = 1.33$$

If we wish to change the design parameters such that we decrease the probability of failure, it is useful to calculate the VIFs from (6.36)

$$\alpha_p^* = \frac{\sigma_p}{\sqrt{\sigma_p^2 + (3\sigma_s)^2}} = \frac{0.8}{\sqrt{0.8^2 + 0.3^2}} = 0.936$$

$$\alpha_s^* = \frac{-3\sigma_s}{\sqrt{\sigma_s^2 + (3\sigma_s)^2}} = \frac{-0.3}{\sqrt{0.8^2 + 0.3^2}} = -0.351$$

The VIFs indicate that the probability of failure is most sensitive to changes in x_p. Let's check this out.

Assume that through an improved manufacturing process, the plastic clip can be manufactured with tighter tolerance such that the standard deviation is cut in half and the steel sheets remain unchanged

$$x_p \sim N(4, 0.4)$$
$$x_s \sim N(1, 0.1)$$

The new probability of failure is found as follows:

$$\beta = \frac{4-3}{\sqrt{0.4^2 + 0.3^2}} = 2$$
$$P_f = \Phi(-2) = 0.0228$$

Which indicates that about 2% of the assemblies will fail which is a substantial improvement over the 12% probability of failure for the original assembly procedure.

Now let us assume that through an improved manufacturing process, the steel sheets can be manufactured with tighter tolerance such that the standard deviation is cut in half and the plastic clip remains unchanged

$$x_p \sim N(4,0.8)$$

$$x_s \sim N(1,0.05)$$

The new probability of failure is found as follows:

$$\beta = \frac{4-3}{\sqrt{0.8^2 + 0.15^2}} = 1.23$$

$$P_f = \Phi(-1.23) = 0.109$$

Which indicates that about 11% of the assemblies will fail which is not a substantial improvement over the 12% probability of failure for the original assembly procedure.

Therefore, it would be wise to address the manufacturing tolerances of the plastic clip if a decrease in the number of assembly failures is desired. Deterministic analysis methods do not allow us to assess the improvements gained through the tighter manufacturing tolerances. Deterministic design analysis would only allow us to change the mean values of the random variables.

We can extend the above example for the generalized linear performance function of the form

$$g(\hat{x}) = a_0 + \sum_{i=1}^{n} a_i x_i \qquad (6.43)$$

The corresponding limit state equation is

$$a_0 + \sum_{i=1}^{n} a_i x_i = 0 \qquad (6.44)$$

If the random variables x_i are independent Gaussian variables with distribution $N(\mu_i, \sigma_i)$, we can transform them into standard normal variables

$$x_i' = \frac{x_i - \mu_i}{\sigma_i}$$

and express the limit state equation as

$$a_0 + \sum_{i=1}^{n} a_i(\sigma_i x_i' + \mu_i) = 0 \qquad (6.45)$$

We know that the distance δ from any surface

$$C_0 + \sum_{i=1}^{n} C_i y_i = 0 \qquad (6.46)$$

to the origin is

$$\delta = \frac{C_0}{\sqrt{\sum_{i=1}^{n} C_i^2}} \qquad (6.47)$$

Writing (6.45) in the form of (6.46) yields

$$\left(a_0 + \sum_{i=1}^{n} a_i \mu_i\right) + \sum_{i=1}^{n} (a_i \sigma_i) x_i' = 0 \qquad (6.48)$$

The safety index β can be expressed as the minimum distance δ by comparing (6.46), (6.47) and (6.48) as

$$\beta = \delta = \frac{a_0 + \sum_{i=1}^{n} a_i \mu_i}{\sqrt{\sum_{i=1}^{n} (a_i \sigma_i)^2}} \qquad (6.49)$$

6.2.2 *General performance function*

So far we have only considered the case of the linear performance function. Now consider the case of generalized performance function of the form

$$g(\hat{x}) = g(x_1, x_2, \cdots, x_n) \quad (6.50)$$

where $\hat{x}$ is the vector or n independent Gaussian random variables. If we replace each random variable x_i by its equivalent standard normal variable

$$\begin{aligned} x_i' &= \frac{x_i - \mu_i}{\sigma_i} \\ x_i &= \sigma_i x_i' + \mu_i \end{aligned} \quad (6.51)$$

the limit-state equation can be written as

$$g(x_1, x_2, \cdots, x_n) = g(\sigma_1 x_1' + \mu_1, \sigma_2 x_2' + \mu_2, \cdots, \sigma_n x_n' + \mu_n) = 0 \quad (6.52)$$

The distance D from any point $\hat{x}' = (x_1', x_2', \cdots, x_n')$ in standard normal space to the origin of standard normal space is

$$D = \sqrt{x_1'^2 + x_2'^2 + \cdots + x_n'^2} = \sqrt{\sum_{i=1}^{n} x_i'^2} \quad (6.53)$$

The MPP of the general performance function (which is the point on the limit-state equation (6.52) closest to the origin) can be found using optimization techniques by minimizing D subject to the constrain that $g(\hat{x}) = 0$.

Lagrangian multipliers may be used for this optimization as

$$L = D + \lambda g(\hat{x}) \quad (6.54)$$

or in scalar form

$$\begin{aligned} L &= \sqrt{\sum_{i=1}^{n} x_i'^2} + \lambda g(x_1) \\ L &= \sqrt{\sum_{i=1}^{n} x_i'^2} + \lambda g(x_2) \\ &\vdots \\ L &= \sqrt{\sum_{i=1}^{n} x_i'^2} + \lambda g(x_n) \end{aligned} \quad (6.55)$$

where (6.55) represents a set of n equations and x_i and x_i' are related according to (6.51). To find the minimum D we minimize L as

$$\frac{\partial L}{\partial x_i'} = 0 \quad i = 1,2,\cdots,n \quad (6.56)$$

and

$$\frac{\partial L}{\partial \lambda} = 0 \quad (6.57)$$

which yields $n+1$ equations with $n+1$ unknowns. The solution will provide $\hat{x}'$ which is the MPP in standard normal space $\hat{x}'^* = (x'^*_1, x'^*_2, \cdots, x'^*_n)$.

Substituting (6.54) into (6.56) yields

$$\frac{\partial L}{\partial x_i'} = \frac{x_i'}{D} + \lambda \frac{\partial g}{\partial x_i'} = 0 \quad i = 1,2,\cdots,n \quad (6.58)$$

from which

$$x_i' = -D\lambda \frac{\partial g}{\partial x_i'} \qquad i = 1,2,\cdots,n \qquad (6.59)$$

Substituting (6.59) into (6.53) yields

$$D = \sqrt{\sum_{i=1}^{n} x_i'^2} = \sqrt{\sum_{i=1}^{n} \left(\lambda D \frac{\partial g}{\partial x_i'} \right)^2}$$

$$D = \lambda D \sqrt{\sum_{i=1}^{n} \frac{\partial g}{\partial x_i'}^2}$$

and therefore,

$$\lambda = \frac{1}{\sqrt{\sum_{i=1}^{n} \frac{\partial g}{\partial x_i'}^2}} \qquad (6.60)$$

Substituting (6.60) into (6.59) yields

$$x_i' = \frac{-D}{\sqrt{\sum_{i=1}^{n} \frac{\partial g}{\partial x_i'}^2}} \frac{\partial g}{\partial x_i'} \qquad i = 1,2,\cdots,n \qquad (6.61)$$

Multiplying each side of the equations in (6.61) as follows,

$$\begin{aligned}
x_1' \frac{\partial g}{\partial x_1'} &= \frac{-D}{\sqrt{\sum_{i=1}^{n} \frac{\partial g}{\partial x_i'}^2}} \frac{\partial g}{\partial x_1'} \frac{\partial g}{\partial x_1'} \\
x_2' \frac{\partial g}{\partial x_2'} &= \frac{-D}{\sqrt{\sum_{i=1}^{n} \frac{\partial g}{\partial x_i'}^2}} \frac{\partial g}{\partial x_2'} \frac{\partial g}{\partial x_2'} \qquad (6.62) \\
&\vdots \\
x_n' \frac{\partial g}{\partial x_n'} &= \frac{-D}{\sqrt{\sum_{i=1}^{n} \frac{\partial g}{\partial x_i'}^2}} \frac{\partial g}{\partial x_n'} \frac{\partial g}{\partial x_n'}
\end{aligned}$$

Summing all of the equations in (6.62) yields

$$\sum_{i=1}^{n} x_i' \left(\frac{\partial g}{\partial x_i'} \right) = \frac{-D}{\sqrt{\sum_{i=1}^{n} \frac{\partial g}{\partial x_i'}^2}} \sum_{i=1}^{n} \frac{\partial g}{\partial x_i'}^2 \qquad (6.63)$$

$$\sum_{i=1}^{n} x_i' \left(\frac{\partial g}{\partial x_i'} \right) = -D \sqrt{\sum_{i=1}^{n} \frac{\partial g}{\partial x_i'}^2}$$

Rearranging terms,

$$D = \frac{-\sum_{i=1}^{n} x_i' \left(\frac{\partial g}{\partial x_i'} \right)}{\sqrt{\sum_{i=1}^{n} \frac{\partial g}{\partial x_i'}^2}} \qquad (6.64)$$

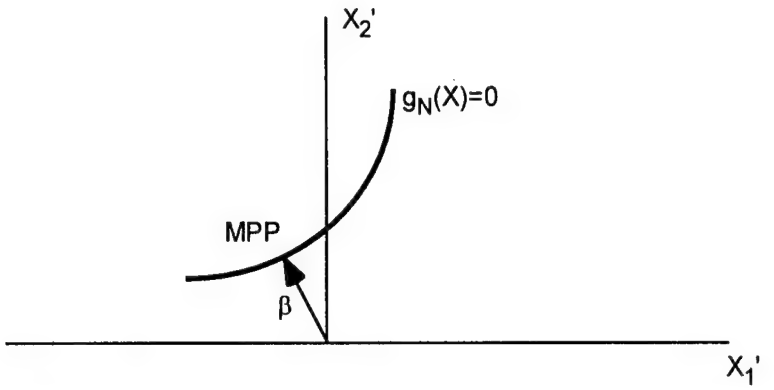

Figure 24: Nonlinear limit state equation in standard normal space.

The minimum distance β is found when D is evaluated at the MPP.

$$\beta = \frac{-\sum_{i=1}^{n} x_i'^{*}\left(\frac{\partial g}{\partial x_i'}\right)_*}{\left(\sqrt{\sum_{i=1}^{n}\frac{\partial g}{\partial x_i'}^2}\right)_*} \quad (6.65)$$

where the subscript * indicates that the expression is numerically evaluated at the MPP. Later, we will present numerical examples to find β using the equations outlined above. Before we do that, however, we should discuss the significance of β for the nonlinear performance function.

Remember that β is the distance from the origin to the MPP in standard normal space for linear limit state equations as shown previously in Figure 22 and nonlinear limit state equations as shown in Figure 24. Recall that in section 6.2.1, we showed that β is the safety index and can be used to find the probability of failure for a linear performance function as

$$P_f = \Phi(-\beta) \quad (6.66)$$

This is an exact equation with no approximations. However, β cannot be used to find the exact probability of failure for a nonlinear performance function. We can use β to approximate the safety index if we consider the following.

Figure 25 compares a linear limit state equation to a nonlinear limit state equation with the same MPP and β. A line along β forms a vector that is perpendicular to the line form by the linear limit state equation $g_L(X) = 0$. Also, the line formed by the linear limit state equation is tangent to the line formed by the

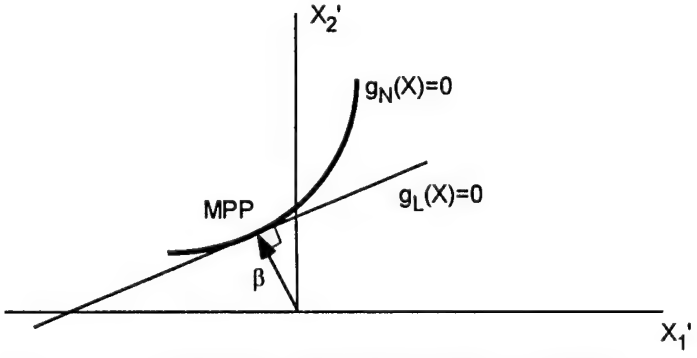

Figure 25: Linear and nonlinear limit state equations in standard normal space.

nonlinear limit state equation $g_N(X) = 0$.

We know from (6.66) that β can be used to find the probability of failure of the linear limit state. The linear limit state is equivalent to a linear approximation to the nonlinear limit state at the MPP. Therefore, β can be used in (6.66) to find the probability of failure for the *first order* approximation of the *high order* limit state. Using β in such a way is the basis for what is know as *first order reliability methods* or FORM. We shall show later that FORM provides good approximations for the probability of failure for most nonlinear limit states. This is primarily because the transformation of the random variables to standard normal variables often serves to rectify or straighten the curve formed by the non-linear limit state equation.

An alternate and much simpler way of deriving the results presented in (6.65) through (6.76) is to first perform a linear approximation to the general limit state equation and then derive an expression for β [20]. We can expand the general nonlinear performance function at the MPP in a Taylor series as

$$g(\hat{x}) = g(\hat{x}^*) + \sum_{i=1}^{n}(x_i - x_i^*)\left(\frac{\partial g}{\partial x_i}\right)_* + \text{HOT} \qquad (6.67)$$

where HOT represents the higher ordered terms in the series expansion. We know that $g(\hat{x}^*) = 0$ because the MPP lies on the failure surface and if we ignore the HOT, then we can write the first ordered approximate to the performance function as

$$g(\hat{x}) = \sum_{i=1}^{n}(x_i - x_i^*)\left(\frac{\partial g}{\partial x_i}\right)_* \qquad (6.68)$$

Recall that $x_i = \sigma_i x_i' + \mu_i$ and therefore we can write

$$x_i - x_i^* = (\sigma_i x_i' + \mu_i) - (\sigma_i x_i'^* + \mu_i) = \sigma_i(x_i' + x_i'^*) \qquad (6.69)$$

and

$$\frac{\partial g}{\partial x_i} = \frac{\partial g}{\partial x_i'}\frac{\partial x_i'}{\partial x_i} = \frac{1}{\sigma_i}\left(\frac{\partial g}{\partial x_i'}\right) \qquad (6.70)$$

Substituting (6.69) and (6.70) into (6.68) yields

$$g(\hat{x}) = \sum_{i=1}^{n}(x_i' - x_i'^*)\left(\frac{\partial g}{\partial x_i'}\right)_* \qquad (6.71)$$

Equation (6.71) is represented by the limit state equation $g_L(X) = 0$ in Figure 25, which is the linear approximation to the general nonlinear limit state equation $g_N(X) = 0$ also shown in Figure 25. Recall that the mean value of the standard normal variable is 0, thus, the mean value of $g(\hat{x})$ is approximated by

$$\mu_g \cong -\sum_{i=1}^{n} x_i'^*\left(\frac{\partial g}{\partial x_i'}\right)_* \qquad (6.72)$$

Recall that the variance of the standard normal variable is 1, thus, the variance of $g(\hat{x})$ is approximated by

$$\sigma_g^2 \cong \sum_{i=1}^{n}\sigma_i^2\left(\frac{\partial g}{\partial x_i'}\right)_*^2 = \sum_{i=1}^{n}\left(\frac{\partial g}{\partial x_i'}\right)_*^2 \qquad (6.73)$$

We know from (6.11) that β is the ratio of the mean value to the standard deviation of $g(\hat{x})$,

$$\beta = \frac{\mu_g}{\sigma_g} = \frac{-\sum_{i=1}^{n} x_i'^*\left(\frac{\partial g}{\partial x_i'}\right)_*}{\sqrt{\sum_{i=1}^{n}\left(\frac{\partial g}{\partial x_i'}\right)_*^2}}$$

which is the same as (6.65).

Remembering that each coordinate of the MPP can be expressed as

$$x_i'^{*} = -\alpha_i^{*}\beta \qquad (6.74)$$

and replacing D with β in (6.61) yields,

$$\alpha_i^{*} = \frac{\left(\frac{\partial g}{\partial x_i'}\right)_{*}}{\left(\sqrt{\sum_{i=1}^{n}\frac{\partial g}{\partial x_i'}^{2}}\right)_{*}} \qquad (6.75)$$

Substituting (6.74) into (6.51) yields

$$x_i^{*} = \mu_i - \alpha_i\sigma_i\beta \qquad (6.76)$$

Equations (6.75) and (6.76) can be used in a numerical algorithm to solve for the MPP as follows [20,21]

1. Assume coordinates for the MPP (usually the mean values of the random variables is a good starting point).
2. Derive each of the derivatives $\frac{\partial g}{\partial x_i'}$.
3. Evaluate each of the derivatives at the assumed coordinates of the MPP.
4. Evaluate each of the direction cosines α_i^{*} according to (6.75).
5. Write each of the coordinates of the MPP x_i^{*} in terms of β according to (6.76).
6. Substitute the x_i^{*}'s found above into the limit state equation $g(\hat{x}) = 0$ such that the limit state equation is in terms of β.
7. Solve for β.
8. Find the updated assumed coordinates of the MPP x_i^{*} by reevaluating (6.76) with the β found above.
9. Repeat steps 3 through 8 until convergence is obtained on β.

There are many other FORM algorithms to solve for β [22]. There are also methods available to find the MPP in real space i.e., no transformation to standard normal space is performed [23]. There are also many other mathematical algorithms available in reliability analysis such as *second order reliability methods* or SORM and direct numerical solutions to the integral shown in (6.6). But, for illustrative purposes, we will use the simple algorithm outlined above.

Numerical Example 6.2: Let us again consider the design of a cantilever beam. Assume the beam is subjected to a point load *w* at the free end. The design criteria specifies that the displacement *d* at the free end does not exceed the a specific value denoted by *z*. From mechanics of materials, we know the performance function describing the end displacement is

$$d = \frac{wL^3}{3EI} \qquad (6.77)$$

where *w* is the load, *L* is the length of the beam, *E* is Young's modulus of the beam material, and *I* is the cross sectional moment of the beam. The limit state that separates the safe region from the failure region is

$$g(\hat{x}) = z - d = z - \frac{wL^3}{3EI} = 0 \qquad (6.78)$$

Assume the deflection criteria *z* is deterministic and set at 0.25 in. Assume the load, length, modulus, and moment are all random variables with the following distributions:

$$\begin{aligned}
\hat{w} &\sim N(\mu_w, \sigma_w) = N(5000,1000) \text{ lbs.} \\
\hat{L} &\sim N(\mu_L, \sigma_L) = N(120,10) \text{ in.} \\
\hat{E} &\sim N(\mu_E, \sigma_E) = N\left(30\text{X}10^6, 0.3\text{X}10^6\right) \text{ psi} \\
\hat{I} &\sim N(\mu_I, \sigma_I) = N(1200,150) \text{ in}^4
\end{aligned} \tag{6.79}$$

The mean deflection according to (6.77) is

$$d = \frac{wL^3}{3EI} = \frac{(5000)(120)^3}{3(30\text{X}10^6)(1200)} = 0.08$$

Following the steps outlined above:

STEP 1: Assume the MPP is at the mean value.

$$\hat{x}^* = (\mu_w, \mu_L, \mu_E, \mu_I) = (5000,120,30\text{X}10^6,1200)$$

STEP 2: Derive each of the derivatives $\frac{\partial g}{\partial x_i'}$.

Considering the random variable w, we can use (6.51) to write (6.78) in terms of w' as

$$g = z - \frac{(\sigma_w w' + \mu_w)L^3}{3EI}$$

and

$$\frac{\partial g}{\partial w'} = \frac{-\sigma_w L^3}{3EI}$$

Considering the random variable L, we can use (6.51) to write (6.78) in terms of L' as

$$g = z - \frac{w(\sigma_L L' + \mu_L)^3}{3EI}$$

and

$$\frac{\partial g}{\partial L'} = \frac{-w3\sigma_L(\sigma_L L' + \mu_L)^2}{3EI} = \frac{-w\sigma_L L^2}{EI}$$

Considering the random variable E, we can use (6.51) to write (6.78) in terms of E' as

$$g = z - \frac{wL^3}{3(\sigma_E E' + \mu_E)I}$$

and

$$\frac{\partial g}{\partial E'} = \frac{-wL^3(-1\sigma_E)}{3(\sigma_E E' + \mu_E)^2 I} = \frac{\sigma_E w L^3}{3E^2 I}$$

Considering the random variable I, we can use (6.51) to write (6.78) in terms of I' as

$$g = z - \frac{wL^3}{3E(\sigma_I I' + \mu_I)}$$

and

$$\frac{\partial g}{\partial I'} = \frac{-wL^3(-1\sigma_I)}{3E(\sigma_I I' + \mu_I)^2} = \frac{\sigma_I wL^3}{3EI^2}$$

STEP 3: Evaluate each of the derivatives at the assumed coordinates of the MPP.

$$\frac{\partial g}{\partial w'} = \frac{-(1000)(120)^3}{3(30\text{X}10^6)(1200)} = -0.016$$

$$\frac{\partial g}{\partial L'} = \frac{-(5000)(10)(120)^2}{(30\text{X}10^6)(1200)} = -0.02$$

$$\frac{\partial g}{\partial E'} = \frac{(0.3\text{X}10^6)(5000)(120)^3}{3(30\text{X}10^6)^2(1200)} = 0.0008$$

$$\frac{\partial g}{\partial I'} = \frac{(150)(5000)(120)^3}{3(30\text{X}10^6)(1200)^2} = 0.01$$

STEP 4: Evaluate each of the direction cosines α_i^* according to (6.75).

$$\alpha_w^* = \frac{-0.016}{\sqrt{0.016^2 + 0.02^2 + 0.0008^2 + 0.01^2}} = \frac{-0.016}{0.0275} = -0.581668$$

$$\alpha_L^* = \frac{-0.02}{0.0275} = -0.727085$$

$$\alpha_E^* = \frac{0.0008}{0.0275} = 0.029083$$

$$\alpha_I^* = \frac{0.01}{0.0275} = 0.363543$$

STEP 5: Write each of the coordinates of the MPP x_i^* in terms of β according to (6.76).

$$w^* = 5000 + (0.582)(1000)\beta = 5000 + 582\beta$$

$$L^* = 120 + (0.727)(10)\beta = 120 + 7.27\beta$$

$$E^* = 30\text{X}10^6 - (0.0291)(0.3\text{X}10^6)\beta = 30\text{X}10^6 - 8730\beta$$

$$I^* = 1200 - (0.364)(150)\beta = 1200 - 54.4\beta$$

STEP 6: Substitute the x_i^*'s found above into the limit state equation $g(\hat{x}^*) = 0$ such that the limit state equation is in terms of β.

$$g(\hat{x}^*) = 0.25 - \frac{(5000 + 582\beta)(120 + 7.27\beta)^3}{3(30\text{X}10^6 - 8730\beta)(1200 - 54.4\beta)} = 0 \qquad (6.80)$$

STEP 7: Solve for β in the above equation.

Equation (6.80) has multiple solutions for β. However, we are usually only interested in values between, say, 5 and –5. A β value between 5 and –5 corresponds to a probability of failure of between 0.0000003 and 0.9999997, which usually covers our range of interest. We can further reduce our range of interest for the beam example by noticing that the mean value of deflection is 0.08 inches and the failure criteria is 0.25 inches. More often than not, the beam deflection will be less than 0.25 inches. We can safely say that the probability of failure is less than 50%. Therefore, we are only interested in positive values of β. Thus, we can restrict our search to β values between 0 and 5.

We can find the solution to (6.80) by trial and error or by plotting $g(\hat{x}^*)$ vs. β as shown in Figure 26. In either case, we find that $\beta = 3.66$.

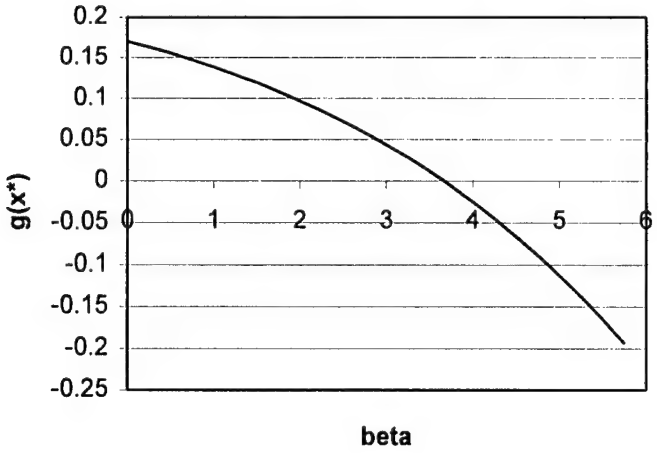

Figure 26: g(x*) as a function of β.

STEP 8: Find the updated assumed coordinates of the MPP x_i^* by reevaluating (6.76) with the α_i's and β found above.

$$w^* = 5000 + (0.582)(1000)(3.66) = 7130$$
$$L^* = 120 + (.727)(10)(3.66) = 146.6$$
$$E^* = 30\text{X}10^6 - (0.0291)(0.3\text{X}10^6)(3.66) = 29.97\text{X}10^6$$
$$I^* = 1200 - (0.0517)(150)(3.66) = 1000$$

STEP 9: Repeat steps 3 through 8 until convergence is obtained on β.

A Summary of the calculations needed to converge on β are shown in

Table 5. The value for *d* shown in the first column of

Table 5 are the most probable failure point found by evaluating (6.77) using the assumed MPP values.

After iteration # 2, the coordinates of the MPP x_i^* are updated by reevaluating (6.76) with the α_i^*'s and β found in iteration # 2. Each of the derivatives is evaluated at the MPP and each of the direction cosines α_i^*'s is reevaluated according to (6.75).

Figure 27 compares the FORM results with Monte Carlo simulation. The beam tip displacements are plotted as a function of the probability of occurrence with standard normal units β. Even though the response function is nonlinear, it can be seen that the FORM results compare very well to the Monte Carlo Simulation, which can be considered the exact solution.

Table 5: Summary of iteration results.

Initial Values Assumed MPP w = 5000 L = 120 E = 30E6 I = 1200 d = 0.08	 Derivative at MPP w = -0.016 L = -0.02 E = 0.0008 I = 0.01	 α_i w = -0.582 L = -0.727 E = 0.291 I = 0.364	 β 3.66
Iteration #1 MPP w = 7130 L = 147 E = 29.97E6 I = 1000 d = 0.2497	 Derivative at MPP w = -0.0350 L = -0.0511 E = 0.00250 I = 0.0375	 α_i w = -0.484 L = -0.705 E = 0.0345 I = 0.517	 β 3.595
Iteration #2 MPP w = 6738 L = 145 E = 29.96E6 I = 921 d = 0.2499	 Derivative at MPP w = -0.0371 L = -0.0516 E = 0.00250 I = 0.0407	 α_i w = -0.491 L = -0.683 E = 0.0331 I = 0.539	 β 3.595
FINAL MPP w = 6766 L = 144 E = 29.96E6 I = 909 d = 0.25	 Derivative at MPP w = -0.0370 L = -0.0519 E = 0.00250 I = 0.0413	 α_i w = -0.487 L = -0.683 E = 0.0330 I = 0.543	

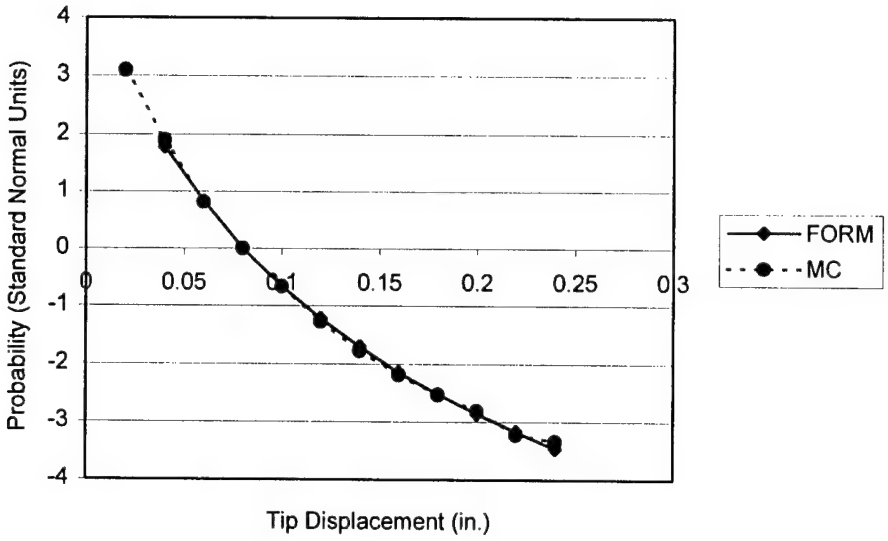

Figure 27: Comparison of FORM results with Monte Carlo simulation.

6.2.3 Mean value methods

Mean value methods are particularly suitable when a closed-form expression of the limit state is not directly available, as is the case when finite element analysis is used to model the structural response. The reliability computation algorithm used in the rotor hub demonstration problem constructs a linear approximation to the limit state in the equivalent standard normal space. Mean value methods works differently, as follows.

1. A first-order Taylor series approximation is constructed at the mean values of the random variables—in the *original space*—based on perturbation-based sensitivity analysis using the finite element analysis or other implicit response models. The two-parameter scheme is used to transform this closed-form approximation and the random variables to the equivalent standard normal space. The Rackwitz-Fiessler [21] iteration formula is used to estimate the MPP, and a first-order estimate of the failure probability is obtained similar to FORM. This is referred to as the mean value first-order (MVFO) estimate.
2. The MVFO estimate is refined using advanced mean value (AMV) analysis. This is simply a deterministic analysis of the system at the MPP, to re-evaluate the g-function. If the MVFO estimate were accurate, the g-function would be exactly zero. If the MVFO estimate were not accurate, then a different value would be obtained for the g-function. The MPP and the probability estimate identified by the MVFO are now assumed to correspond to this new value of the g-function.
3. The above two steps are repeated for different values of the g-function. This results in the construction of the CDF of the g-function.

Mean value methods are a practical alternative to FORM, if the deterministic analysis of the system is expensive. By simply combining the information from the MVFO step and one additional deterministic analysis, one is able to obtain a substantially improved estimate of the failure probability.

There are optimization algorithms, such as BEGS, which combine the information in the iteration steps to perform an accurate search. Such algorithms are especially useful when the Rackwitz-Fiessler algorithm fails to converge. However, the programming effort and the memory storage requirements in these methods, plus the marginal improvement in accuracy over the Rackwitz-Fiessler method have hindered their widespread

application in structural reliability studies. The AMV, with its minimal one step combination, is a practical approach in this direction.

The AMV estimate can be further improved with more iteration. In the AMV + method, sensitivity analysis is performed after the AMV step, and steps 1 and 2 of the above procedure are repeated. In a similar manner, further iterations can be done to produce AMV + +, AMV + + +, etc., estimates. In each case, note that only the first iteration (MVFO) and the latest deterministic analysis are combined. It is important to note here that the sensitivity information in the AMV is computed only in the first iteration, i.e., at the MVFO step, which is at the mean values of the random variables. If the sensitivity values are needed at the MPP, then full sensitivity analysis needs to be performed.

The AMV method approximates the *g* function at the very beginning (at the mean values of the random variables). That is, the first-order derivatives are calculated at the beginning using finite difference or perturbation analysis to have a first-order Taylor series approximation as shown below

$$g(\vec{X}) \approx g(\vec{x^*}) + \sum_{i=1}^{n} \frac{\partial g}{\partial x_i^*}(x_i - x_i^*) \tag{6.81}$$

where $\vec{x^*}$ represents the expansion point. Notice that the linear approximation of Eq. (6.81) does not involve mixed terms, and the effects of the random variables on the g-function are considered separately. This introduces additional approximations.

Numerical Example 6.3: Assume we have a cantilever bean of length *L*, loaded at the free end with a force *w*. We wish to find the vertical displacement at the free end of the beam. We know that the load *w*, stiffness *E*, and the moment of inertia *I*, are all normally distributed random variables, with mean and standard deviation as follows:

$$w \approx N(5000,1000) \text{ lbs}$$
$$L \approx N(120,10) \text{ in}$$
$$E \approx N(30\times10^6, 0.3\times10^6) \text{ psi}$$
$$I \approx N(1200,150) \text{ in}^4$$

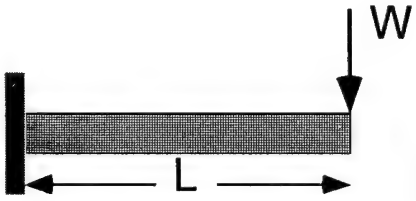

Figure 28: Cantilever beam loaded at the free end.

We know from mechanics that the vertical displacement *d* of the free end of a beam is

$$d = \frac{wL^3}{3EI} \tag{6.82}$$

Let us assume , for this example, we could not determine the displacement in closed form and had to use the simple finite element model in Figure 28 to determine the end displacement. The details of each step involved in performing a Mean Value First Order (MVFO) analysis for the above example are enumerated below.

MVFO Analysis

Step 1. The first step in a MVFO analysis is performing a perturbation analysis about the mean values of the input random variables (*w, L, E, I*) using the finite element model, to determine the vertical tip displacement *d*, of the cantilever beam. The perturbation analysis involved changing each variable by one-tenth of its standard deviation about its mean value and rerunning the finite element model to create the array of five finite element runs as shown below. The results of the perturbation analysis are shown in Table 6.

Table 6: Perturbation analysis

w	*L*	*E*	*I*	*d (FEM)*
5000	120	3.00E+07	1200	8.00E-02
5100	120	3.00E+07	1200	8.16E-02
5000	121	3.00E+07	1200	8.20E-02
5000	120	3.00E+07	1200	7.99E-02
5000	120	3.00E+07	1215	7.90E-02

Step 2. Based on the perturbation analysis of Step 1, a first order Taylor Series expansion is performed about the mean values of the random variables using equation (6.81), expressing the vertical tip displacement *d*, as a function of the input variables. Equation (6.83) represents this linear functional relationship. Comparing equations (6.82) and (6.83), it should be noted that equation (6.83) is only an approximate relationship based on finite element analysis at the mean value of the random variables.

$$d_{approx} = -0.0831 + 1.6*10^{-5} w + 2.1*10^{-3} L - 2.66*10^{-9} E - 6.58*10^{-5} I \qquad (6.83)$$

Step 3. Having defined equation (6.83), the next step is to define the limit state equation for first order reliability analysis. The limit state equation is defined as:

$$g \equiv d_0 - d_{approx} \qquad (6.84)$$

where d_0 is the "level of displacement" for which the reliability analysis is performed. In other words, the reliability analysis will find the probability that the beam displacement d_{approx} is greater than d_0.

Based on a range of values of d_0, the probability that $g \leq 0$ was determined. Table 7 lists the range of values of d_0 considered along with the corresponding reliability indices (β) and the most probable values (MPP) of the input random variables (*w, L, E, I*) for which the relationship $g \leq 0$ was satisfied. Figure 29 plots d_0 vs. β for the MVFO analysis which represents the cumulative distribution function (CDF) of the vertical tip displacement *d* of the beam. Notice that the MVFO curve is linear. This is because the random variables are normal and a linear approximation to the beam displacement response (equation (6.83)) was used in the analysis. However, we have no reason to believe that the true displacement response of the beam is linear. If we wish to develop a better approximation to the true CDF, we perform an advanced mean value analysis.

Table 7: MVFO results

d_0	β	*w**	*L**	*E**	*I**	d_{FEM}
0.00	3.20E+00	3.19E+03	9.62E+01	3.00E+07	1.37E+03	0.023
0.02	2.49E+00	3.59E+03	1.01E+02	3.00E+07	1.33E+03	0.031
0.04	1.78E+00	4.00E+03	1.07E+02	3.00E+07	1.29E+03	0.042
0.06	1.07E+00	4.39E+03	1.12E+02	3.00E+07	1.26E+03	0.055
0.08	3.60E-01	4.80E+03	1.17E+02	3.00E+07	1.22E+03	0.070
0.10	-3.50E-01	5.20E+03	1.23E+02	3.00E+07	1.18E+03	0.091
0.12	-1.06E+00	5.60E+03	1.28E+02	3.00E+07	1.14E+03	0.114
0.14	-1.77E+00	6.00E+03	1.33E+02	3.00E+07	1.11E+03	0.142
0.16	-2.48E+00	6.41E+03	1.38E+02	3.00E+07	1.07E+03	0.175
0.18	-3.19E+00	6.81E+03	1.44E+02	3.00E+07	1.03E+03	0.219
0.20	-3.90E+00	7.21E+03	1.49E+02	3.00E+07	9.95E+02	0.266

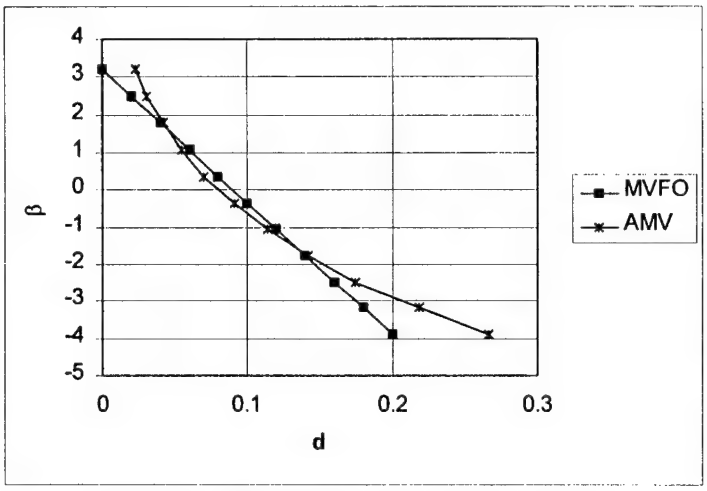

Figure 29: MVFO and AMV analysis results.

AMV Analysis

AMV is a continuation of the MVFO analysis in which we use the MPP from the MVFO analysis and the finite element model to further refine the reliability analysis.

Step 4. The vertical tip displacement based on the performing a finite element analysis using the MPP values of the random variables (columns 3 through 6 of Table 7) is evaluated. These values are listed in the last column of Table 7. Notice that the value of the tip displacement from the finite element analysis d_{FEM} is not the same as d_0. The value of d_0 is equivalent to the value obtained by using the approximate equation (6.83) at the MPP. The displacement value at each β is shifted from d_0 to d_{FEM} as show by the AMV curve in Figure 29. The AMV curve is the CDF that represents a refinement to the MVFO CDF using just one additional finite element run at each value of β.

A Monte Carlo simulation was performed using the closed-form response (equation (6.82)) for comparison purposes. Figure 30 compares the AMV results with Monte Carlo simulation. The comparison shows excellent agreement between the two methods. However, we must remember that the purpose behind performing mean value methods is because we do not have closed-form solutions available and have to use computational models to determine the response of interest. Therefore an AMV+ analysis can be performed to verify the validity of the AMV analysis.

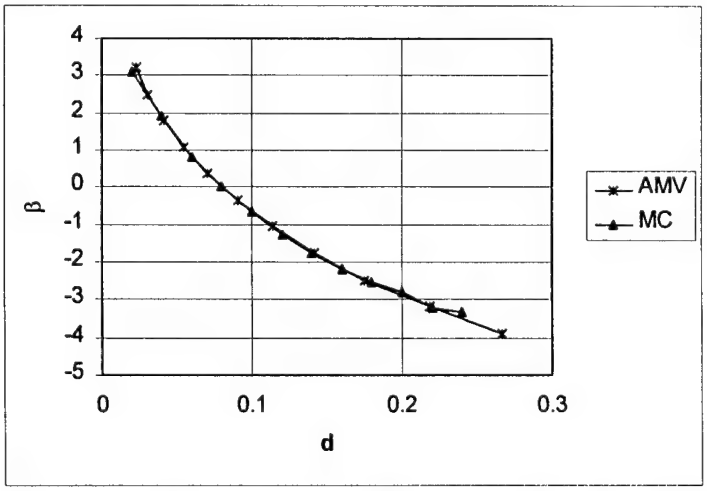

Figure 30: Comparison of AMV results to Monte Carlo.

AMV+ Analysis

AMV+ is a continuation of the AMV analysis in which we use the MPP from the MVFO/AMV analysis and the finite element model to further refine the reliability analysis.

Step 5. If we are interested in further refining the AMV estimate at the β value of -3.19 (refer Table 7), for example, we perform another perturbation analysis by repeating Steps 1 and 2. The only difference this time is the perturbation analysis is now performed about the MPP values of the input random variables at β=-3.19 as opposed to the mean values in the MVFO analysis. The results of the perturbation analysis are shown in Table 8.

Table 8: AMV+ perturbation analysis

w^*	L^*	E^*	I^*	d
6.81E+03	1.44E+02	3.00E+07	1.03E+03	2.19E-01
6.91E+03	1.44E+02	3.00E+07	1.03E+03	2.22E-01
6.81E+03	1.45E+02	3.00E+07	1.03E+03	2.23E-01
6.81E+03	1.44E+02	3.00E+07	1.03E+03	2.18E-01
6.81E+03	1.44E+02	3.00E+07	1.05E+03	2.16E-01

Step 6. Based on the above perturbation analysis a first order Taylor series expansion (equation (6.81)) is performed about the MPP as shown in equation (6.85).

$$d_{approx_{AMV+}} = -0.2266 + 3.21*10^{-5} w + 4.588*10^{-3} L - 7.28*10^{-9} E - 2.1*10^{-4} I \qquad (6.85)$$

Step 7. The limit state equation is defined as follows. d_{AMV} is chosen as 0.219 because at the AMV step for β = -3.19 the d value from Finite Element Analysis was 0.219 (refer Table 7)

$$\begin{aligned} g &\equiv d_{AMV} - d_{approx_{AMV+}} \\ &\equiv 0.219 - d_{approx_{AMV+}} \end{aligned} \qquad (6.86)$$

Step 8. Performing a first order reliability analysis with equation (6.86) as the limit state yields the following results.

d_{AMV}	β	w^*	L^*	E^*	I^*	d_{FEM}
0.219	-3.41E+00	6.72E+03	1.44E+02	3.00E+07	9.46E+02	0.236

Figure 31 compares the AMV+ result with the AMV results. It can bee seen that the AMV+ result compares favorably with the AMV results and thus it can be assumed that the AMV and AMV+ results are valid in the regime of β = -3.

6.2.4 Direct FORM

If we repeat steps 1 through 8 the analysis would be known as AMV++. If we again repeat the steps the analysis is known as AMV+++ and so on. If we perform the analysis in which the number of repetitions is based on the convergence of β and/or the MPP, the analysis is known as *direct FORM*. Therefore MVFO and AMV methods are subsets of the direct FORM analysis.

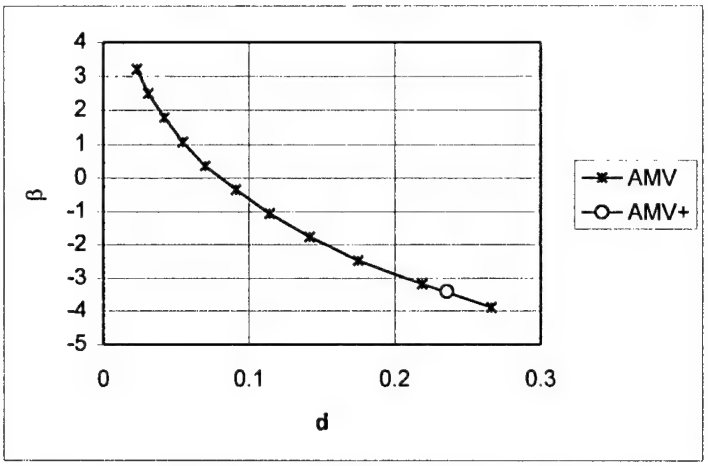

Figure 31: Comparison of AMV results and AMV+ results.

6.3 Design of Experiments Input Matrix

Response surface methods require an analytical relationship that describes the component behavior subject to a specific failure mechanism. In cases where explicit relationships describing system degradation or loading exist, they can be used by probabilistic methods to predict reliability and life. However, if computational methods, such as finite element methods, are employed to estimate component loading or behavior, the functional relationship between loading and design variables must be approximated using closed-form equations.

Response surface methods calculate implicit functions describing component behavior. In order to estimate the response surface, several steps are involved, namely:

1. *Identifying the significant random variables.*
2. *Establishing the degree of model fidelity required or desired.* The engineer must determine if a first-order linear model description of the phenomena is sufficient or if a higher order model is required.
3. *Determining the experimental design.* The experimental design must be constructed based on the model that must be fitted, the number of experimental conditions that can be tested, time constraints and budget constraints. In addition, the number of levels for each variable must be determined (i.e.: how many different values of each variable will be tested).
4. *Executing the experimental design.* The computational software should be run at the individual variable settings (experimental runs) determined by the experimental design, with the variable settings and resulting output recorded.
5. *Fitting the response surface model.* Multiple regression techniques are used to estimate the parameters of the approximating polynomial. Typically, first or second-order models of the response surface are sufficient.

The selection of the model order is fairly straightforward. Unless evidence or knowledge exists to the contrary, a second-order design is desirable since first-order effects are included, as well as measures of curvature. If a second-order response surface does not sufficiently fit the computational model, then higher-order designs can be implemented.

A critical consideration is the number of computational model conditions that must be executed in order to establish a valid response surface model of the phenomena of interest. Minimizing the number of experimental conditions that must be modeled can drastically reduce the computational time required. While fractional factorial designs, such as resolutions III, IV, and IV designs, might seem to offer the most economical means of determining the response surface, they are not the most efficient designs available.

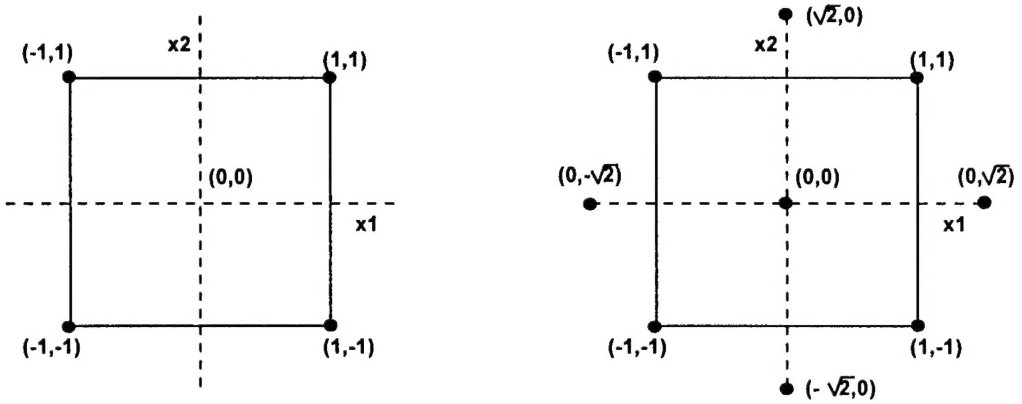

Figure 32: CCD treatments for 2k design (left) and axial runs (right).

In selecting the experimental design for fitting a response surface the desirable features are:

1. A reasonable distribution of data points throughout the design space.
2. Enables experiments to be performed in blocks to reduce error and noise.
3. Generates estimates of error for the fitted model.
4. Economizes the number or runs.
5. Does not require a large number of levels of the variables.
6. Enables determination of model adequacy, especially estimation of lack of fit of the model.
7. Allows designs of higher order to be built upon sequentially.

Although fractional factorial design reduce the number of combination treatments required, they require repetition of the treatments in order to obtain error estimates for the fitted relationships. In contrast, experimental design tailored to fitting response surfaces can reduce the required number of treatments and the number of required repetitions. If the factors under investigation are to be explored at two levels then central composite designs (CCD) have several advantages. First, CCD enables the adoption of sequential experimentation. In this case a 2k design of resolution V is used to fit a first-order model, which exhibits a statistically significant lack of fit. The experiment then progresses with additional treatments to include 2k axial runs. A graphical depiction of the treatments run in the CCD case is shown for 2 variables in Figure 32. In this case the initial runs are conducted at factor level settings of (1,1), (1,-1), (-1,1), and (-1,-1) for the two factors. If following the initial runs the fitted first-order model lacks fit, additional runs are conducted at 5 additional treatments, specifically, (0,0), (0,$\sqrt{2}$), (0,-$\sqrt{2}$), ($\sqrt{2}$,0), and (-$\sqrt{2}$,0) [see Figure 32]. The axial treatments [(0,$\sqrt{2}$), (0,-$\sqrt{2}$), ($\sqrt{2}$,0), (-$\sqrt{2}$,0)] can involve a single replication, but numerous trials are typically conducted at the center point (0,0). The addition of center point runs allows for the estimation of curvature effects, while axial points enable estimation of quadratic terms. Thus the resolution V fractional design allows estimation of the linear and 2-factor interaction terms, and is variance optimal for these terms. The axial points enable estimation of quadratics terms, since without them only pure second order terms are estimated. Center run points provide estimates of error and improve quadratic term estimation.

Where models are to be fit to factors that have three levels, the CCD approach is not applicable. In cases of factors with three levels are investigated, Box-Behnken designs (BBD) [24] are efficient methods to fit response surfaces. Combining 2k factorial incomplete block designs forms the BBD. Examining the Box-Behnken design for three variables in Figure 33, it can be seen that it is a spherical design, with no points at the upper or lower variable limits (i.e.: no points at the vertices). This can be advantageous if cost or physical constraints make conducting tests at extreme variable levels infeasible.

There are other advantages to using design specifically tailored to generating response surface in addition to that of sequential experimentation. A significant consideration in design selection is that of rotatability. Design rotatability exists when $N\,Var\ y(x)/\sigma^2$ is constant for all locations equidistant from the center of

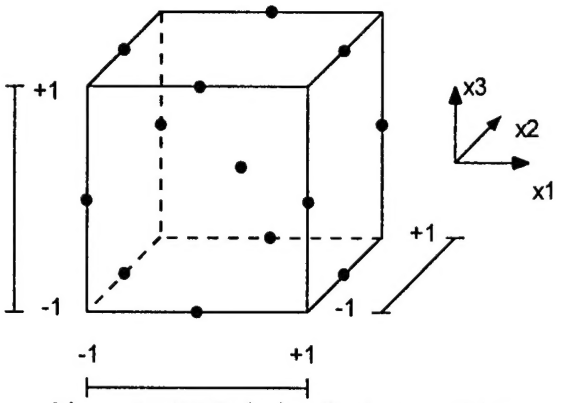

Figure 33: BBD design for three variables.

the design. The impact of rotatability is that for any two points, x_1 and x_2 that have the same distance from the center, their associated predicted values, $y(x_1)$ and $y(x_2)$, have the same variance. Thus if the design is rotated about the center the variance of the predicted y is unchanged. The implication of rotatable designs is that all predicted response values are equally uncertain at any given radius from the center. If non-rotatable designs are used, the resulting response surface could have a bias in the variance depending on both the distance from the center and the factor levels. The benefits rotatability are significant, favoring the use of either rotatable central composite or Box-Behnken designs for establishing the treatment array for the experiments.

7 Phase I Conclusion

Phase I of the proposed research effort has successfully demonstrated that the probabilistic analysis framework can be integrated with current state-of-the-art composite design to estimate the failure probability due to various critical failure modes. In addition, the same framework can be used to compute the sensitivity of the various random input design parameters to the final design without any extra computational effort.

In particular, a composite helicopter rotor hub test specimen, subjected to cyclic loading, was analyzed to predict delamination onset failure. A structural model of the rotor hub was created using the finite element program ANSYS. The output from the structural analysis in ANSYS was fed into the Virtual Crack Closure Technique (VCCT) module to model delamination onset. A Reliability Analysis framework including Response Surface Analysis and FORM modules was developed to integrate with the structural analysis modules. The response surface analysis was used to develop a limit state equation relating the primitive input design parameters (random variables such as *E, P*, and Φ) to strain energy release rate G_{max}. FORM analysis estimated the probability of delamination onset and furthermore, determined the distribution of the failure probability over a range of cyclic lives. In addition, the sensitivity analysis in FORM revealed that the external loading to the structure, namely *P* and Φ are the most critical parameters affecting the reliability of the rotor hub. Summarizing, the following tasks will be completed at the end of Phase I.

- Demonstrated probabilistic analysis framework
- Demonstrated composite Finite Element modeling (FEM) technique
- Developed framework for integrating probabilistic and FEM codes
- Applied developed method to a practical problem

Figure 34 further helps in illustrating the tasks accomplished in the Phase I effort and how these tasks fit into the complete Phase II effort. The solid boxes in Figure 34 represent the tasks that were successfully completed at the end of Phase I. The hatched boxes in the figure represent the tasks that are proposed in Phase II to develop a powerful, commercially viable composite analysis design tool.

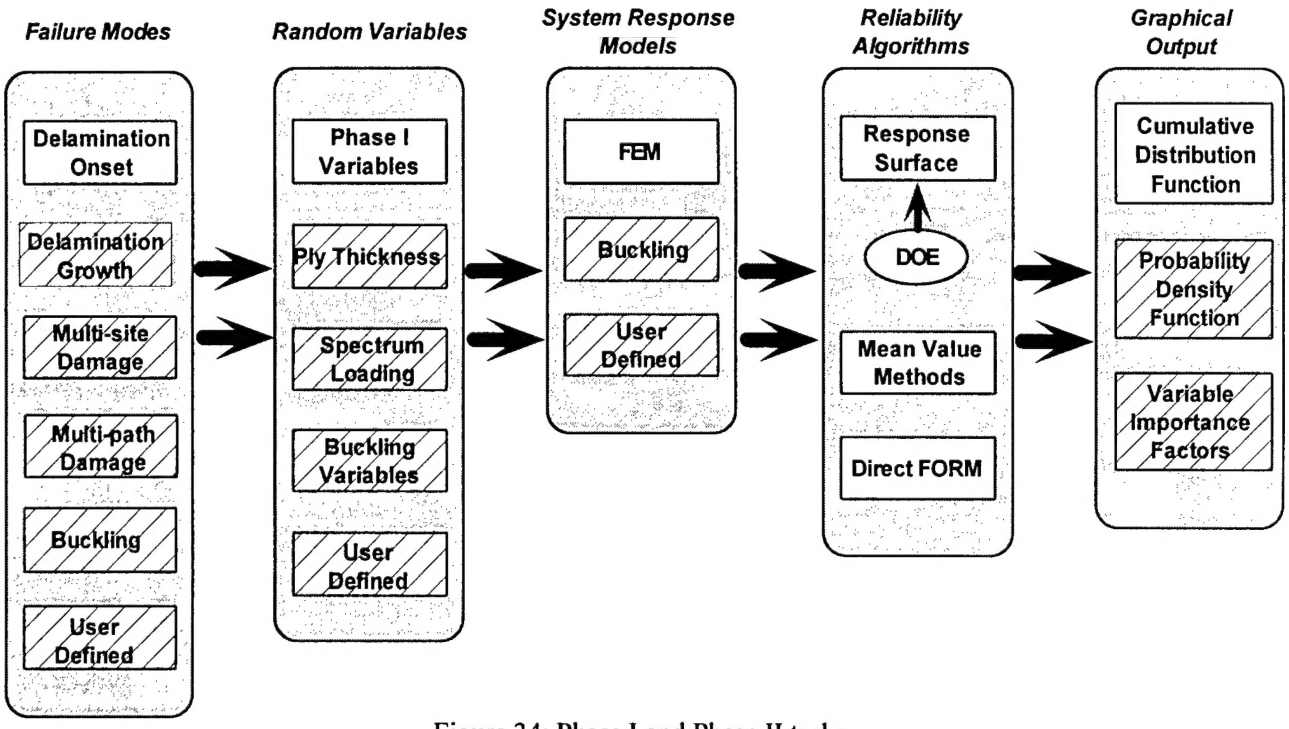

Figure 34: Phase I and Phase II tasks.

8 References

[1] Everett, R.A., Bartlett, F.D., Elber, W., **Probabilistic Fatigue Methodology for Six Nines Reliability**, NASA Tech Memo 102757, 1990.

[2] Fish, J. C., and Lee, S. W., "Tensile Strength of Tapered Composite Structures", AIAA Paper No. 88-2252, Proceedings of the 30th AIAA/ASME/ASCE/AHS SDM Conference, Williamsburg, VA, pp. 324-333, 1988.

[3] Hoa, S. V., Daoust, J., and Du, B.L., "Interlaminar Stresses in Tapered Laminates", **Polymer Composites**, Vol. 9, No. 5, pp. 337-344, 1988.

[4] Llanos, A. S., Lee, S. W., and Vizzini, A. J., "Delamination Prevention in Tapered Composite Structures under Uniaxial Tensile Loads", AIAA Paper No. 90-1063, Proceedings of the 31st AIAA/ASME/ASCE/AHS SDM Conference, Long Beach, CA, pp. 1242-1252, 1990.

[5] Hoa, S. V., Daoust, J., "Parameters Affecting Interlaminar Stresses in Tapered Laminates Under Static Loading Conditions", **Polymer Composites**, Vol. 10, No. 5, pp. 374-383, 1989.

[6] Kemp, B. L., and Johnson, E. R., "Response and Failure Analysis of a Graphite-Epoxy Laminate Containing Terminating Internal Plies", AIAA Paper No. 85-0608, Proceedings of the 26th AIAA/ASME/ASCE/AHS SDM Conference, Orlando, FL, pp. 13-24, 1985.

[7] Curry, J. M., Johnson, E. R., and Starnes, J. H., "Effect of Dropped Plies on the Strength of Graphite Epoxy Laminates", Proceedings of the 29th AIAA/ASME/ASCE/AHS SDM Conference, Monterey, CA, pp. 737-747, 1987.

[8] Murri, G. B., Salpekar, S. A., and O'Brien, T. K., "Fatigue Delamination Onset Prediction in Unidirectional Tapered Laminates", **Composite Materials: Fatigue and Fracture** (3rd Vol.), ASTM STP 1110, T. K. O'Brien, Ed., ASTM, Philadelphia, pp. 312-339, 1991.

[9] Winsom, M. R., "Delamination in tapered Unidirectional Glass Fibre-Epoxy Under Static Tension Loading", AIAA Paper No. 91-1142, Proceedings of the 32nd AIAA/ASME/ASCE/AHS SDM Conference, Baltimore, MD, pp. 1162-1172, 1991.

[10] Trethewey, B. R., Jr; Gillespie, J. W., Jr; and Wilkins, D. J., "Interlaminar Performance of Tapered Composite Laminates", Proceedings of the American Society for Composites, 5th Technical Conference, East Lansing, MI, pp. 361-372, 1990.

[11] Armanios, E. A., and Parnas, L., "Delamination Analysis of Tapered Laminated Composites under Tensile Loading", **Composite Materials: Fatigue and Fracture** (3rd Vol.), ASTM STP 1110, T. K. O'Brien, Ed., ASTM, Philadelphia, pp. 340-358, 1991.

[12] Salpekar, S. A., Raju, I. S., and O'Brien, T. K., "Strain Energy Release Rate Analysis of Delamination in a Tapered Lamiante Subjected to Tension Load", Proceedings of the American Society for Composites, 3rd Technical Conference, Seattle, WA, pp. 642-654, 1988.

[13] Murri, G. B., O'Brien, T. K., and Salpekar, S. A., "Tension Fatigue of Glass/Epoxy and Graphite/Epoxy Tapered Laminates" **Journal of the American Helicopter Society**, Vol. 38, No. 1, pp. 29-37, 1993.

[14] O'Brien, T. K., Murri, G. B., Hagemeier, R., and Rogers, C., "Combined Tension and Bending testing of Tapered Composite Laminates", **Applied Composite Materials**, Vol, 1, No. 6, pp. 401-413, 1995.

[15] Murri, G. B., O'Brien, T. K., and Rousseau, C. Q., "Fatigue Life Prediction of Tapered Composite Laminates", American Helicopter Society, 53rd Annual Forum, Apr-May, 1997, Virginia Beach, VA.

[16] Rybicki, E. F., and Kanninen, M. F., "A Finite Element Calculation of Stress-Intensity Factors by a Modified Crack-Closure Integral", **Engineering Fracture Mechanics,** Vol. 9, pp. 931-938, 1977.

[17] Raju, I. S., "Calculation of Strain Energy Release Rates with Higher Order and Singular Finite Elements", **Engineering Fracture Mechanics,** Vol. 28, pp. 251-274, 1987.

[18] Matthews, F.L., and Rawlings, R.D., **Composite Materials: Engineering and Science**, Chapman and Hall, London, 1994.

[19] Madsen. H.O., S. Krenk, and N.C. Lind, **Methods of Structural Safety**, Prentice-Hall, Englewood Cliffs, NJ, 1986.

[20] Ang, A. H.-S., and Tang, W. H., **Probability Concept in Engineering Design, Vol. II: Decision, Risk, and Reliability**, J Wiley & Sons, New York, 1984.

[21] Rackwitz, R. and Fiessler, B., *Structural Reliability Under Combined Random Load Sequences*, **Comput. Struct.**, 9: pp. 484-494 1978.

[22] Aerospace Information Report 5080, **Integration of Probabilistic Methods into the Design Process,** SAE, Warrendale, PA, 1997.

[23] Lin, H.-Z, Khalessi, M. R., *Identification of the Most-Probable-Point in Original Space,* Proceedings of the 34th AIAA/ASME/ASCE/AHS SDM Confernece, pp. 1154-1162, 1993.

[24] Box, G. E. P., Behnken, D. W., *Some New Three Level Designs for the Study of Quantitative Variables,* Technometrics, Vol. 2, pp. 455-475, 1960.